Zain Publications
Company Registration No: UAN TS02E0015729
(Govt. of India, Ministry of Micro, Small & Medium Enterprises)
Contact Person: Dr. Mohd Zainuddin
Address: #12-1-898, North Lalaguda, Secunderabad, Telangana, India

IJRIT

Ngesa Joel Ochola, International Journal of Robotics and Information Technology, Volume 1, Issue 2, Dec 2017, Pg: 74-103

Dynamics of MHD Heat and Mass Transfer Past a Semi-Infinite Vertical Porous Plate in a Turbulent Boundary Layer

Ngesa Joel Ochola
Machakos University
Email: ngjs9@yahoo.com

Abstract: ***This study addresses the problem of unsteady free convection incompressible MHD fluid flow past a semi-infinite vertical porous plate in the presence of a strong magnetic field inclined at an angle θ to the plate with Hall and Ion-Slip currents in a Turbulent boundary layer. The partial differential equations governing the flow problem considered in our study are solved by a finite difference approximation. The effects of modified Grashof number, suction velocity, the angle of inclination, time, Hall current, Ion-Slip current, Schmidt number and heat source parameter on the convectively cooled or convectively heated plate restricted to turbulent boundary layer is considered. The results show that the Hall current, Schmidt number, Modified Grashof number, heat source parameter, suction velocity, time, angle of inclination, Ion-Slip current on the convectively cooled or convectively heated plate affect the velocity, temperature and concentration profiles. Increases in Hall parameter cause a decrease in both primary and secondary profiles while increase in Ion Slip current parameter leads to increase in primary velocity profiles but a decrease in secondary velocity profiles.***
Keywords: Free Convection, MHD, Turbulent flow, Semi-infinite plate, Hall and Ion-Slip currents

INTRODUCTION

MHD studies the motion of electrically conducting fluid in the presence of a magnetic field. This motion leads to induced electric currents on which mechanical forces are exerted by magnetic field. The induced electric currents in turn produce induced magnetic field which affect the original magnetic field.

The electrical current density $\vec{J}$ represents the relative motion of charged particles in a fluid. The equation of electric current density may be derived from the diffusion velocities of the charged particles. The major forces on charged particles are electromagnetic forces. If we consider only the electromagnetic forces, we may obtain the generalized Ohm's law. However the deduction from the diffusion velocity of charged particles is more complicated than the generalized Ohm's law. When electric field $\vec{E}$ is applied, there will be an electric current in the direction of $\vec{E}$. If the magnetic field $\vec{H}$ is perpendicular to $\vec{E}$, there will be an electromagnetic force $\vec{J} \times \vec{B}$, which is perpendicular to both $\vec{E}$ and $\vec{H}$, which is known as Hall current. For the same electromagnetic force, the motion of ions is different from that of electrons, when the electromagnetic force is very large (such as in a very strong magnetic field) the diffusion velocity of ions cannot be neglected. If we consider the diffusion velocity of ions as well as that

Zain Publications
Company Registration No: UAN TS02E0015729
(Govt. of India, Ministry of Micro, Small & Medium Enterprises)
Contact Person: Dr. Mohd Zainuddin
Address: #12-1-898, North Lalaguda, Secunderabad, Telangana, India

of electrons, we have the phenomenon of Ion-slip current.

In turbulent flow, the transport mechanism is aided by innumerable eddies. Irregular velocity fluctuations are superimposed upon the motion of the main stream, and these fluctuations are primarily responsible for the transfer of heat as well as momentum.

The fluid motion may be caused by external mechanical means for example by a fun, pumps, in which case the process is called forced convection. If the fluid motion is caused by density differences which are created by the temperature differences existing in the fluid mass, the process is called free convection or natural convection. In natural convection, flow velocities are produced by the buoyancy forces only; hence there are no externally induced flow velocities. As a result, the Nusselt number doesn't depend on Reynolds number.

Buoyant force causes denser parts of the fluid to move downwards and less dense parts to move upwards. The density differences can result from various effects such as differences in concentration of dissolved matter or in temperature.

Typical examples of turbulent flows are flow around, as well as in cars, Aeroplanes and buildings.

Bo Lu et al. (2013) did a study on three dimensional MHD simulation of the electromagnetic flow meter for laminar and turbulent flows, their Numerical results show that induced electric potential difference at the electrodes agreed with the theoretical values. Simulations also render the detailed distributions of induced electric field, current density, electric potential and induced magnetic field. Buffetta G. et al. (2012) in their paper, the ultimate state of thermal convection in Reyleigh-Taylor turbulence, discusses the so-called ultimate state of thermal convection, first proposed by Kraichnan almost 50 years ago and recently observed in numerical simulations of turbulent convection in the absence of boundaries. They focus on numerical simulations of turbulence generated by the Rayleigh–Taylor instability in a wide range of Rayleigh and Prandtl numbers and results point out to the conclusion that RT turbulence provides a natural realization of the ultimate state of thermal convection thus highlighting the relationship between the absence of boundaries and the emergence of the ultimate state scaling for global statistical quantities.

Sanvincente E et al. (2013) had an experimental study on natural convection flows in a differentially heated open channel configuration. The applications concern the free cooling of both the photovoltaic components integrated within the building envelope (double-skin configuration) and the building itself. Particular focus is given to the identification of integration configurations favorable to both heat transfer on the rear side of components and buoyancy enhancement. The test section consists of a vertical channel with two walls composed of different heating modules. In the present investigation the thermal configuration considers one wall heated uniformly while the other is not heated. They focus on the kinematic characteristics of the flow and convective heat transfer at the heated wall. The experimental evidence shows that

the flow is neither really turbulent nor purely laminar for the range of Rayleigh numbers considered. Although the average characteristics of the flow seem perfectly consistent with the results obtained, changes of behavior seem to occur intermittently.

Mohammad Zoynal Abedin et al. (2012) carried out study on turbulence characteristics and vertical structures in combined convection boundary layers along a heated vertical flat plate, They performed Time-developing direct numerical simulations for the combined-convection boundary layers created by imposing aiding and opposing free streams to the pure natural-convection boundary layer in air along a heated vertical flat plate to clarify their structural characteristics. The numerical results reveal that with a slight increase in free stream velocity, the transition region moves downstream for aiding flow and upstream for opposing flow. Mathew Kinyanjui et al. (2012) investigated a turbulent flow of a rotating system past a semi-infinite vertical porous plate. They considered the flow in the presence of a variable magnetic field. They noted that the Hall current, rotation, Eckert number, injection and Schmidt number affect the velocity, temperature and concentration profiles.

Yasuo Hattori et al. (2006) did investigate on the turbulence characteristics of a natural-convection boundary layer in air along a vertical plate heated at high temperatures experimentally. In their study two-dimensional velocity vectors and instantaneous temperature in the boundary layer at a wall temperature up to 300 ℃ are measured using a particle image velocimetry and a cold wire found that heat transfer rates even for a wall temperature of 300 ℃ are well expressed by an empirical formula obtained for low wall temperature and the region of transition from laminar to turbulence does not change much with an increase in wall temperature. In addition, the profiles of turbulent quantities measured at a wall temperature of 300 ℃ resemble those observed at low wall temperatures, and thus the effects of high heat on the turbulent behavior in the boundary layer are quite small. The measured velocity vectors and the higher-order statistics, such as skewness and flatness factors of fluctuating velocities and temperature, also suggest that the structure of large-scale fluid motions in the outer layer of the natural-convection boundary layer, closely connected with turbulence generation, is maintained even under high wall temperature conditions.

Specific equations governing fluid flow

The equations governing incompressible unsteady free convection fluid flow in the presence of heat and mass transfers are considered. In this study unsteady free convection magnetohydrodynamic flow past a semi- infinite vertical porous plate subjected to a strong magnetic field inclined at an angle of θ to the plate and constant suction is studied. The $x^* - axis$ is taken along the plate in vertically upward direction, which is the direction of flow.

Zain Publications
Company Registration No: UAN TS02E0015729
(Govt. of India, Ministry of Micro, Small & Medium Enterprises)
Contact Person: Dr. Mohd Zainuddin
Address: #12-1-898, North Lalaguda, Secunderabad, Telangana, India
Ngesa Joel Ochola, International Journal of Robotics and Information Technology, Volume 1, Issue 2, Dec 2017, Pg: 74-103

The z^*- axis taken normal to the plate, since the plate is semi- infinite in length and for a two dimensional free convective fluid flow the physical variables are functions of $x*, z*$ *and* t^*. The fluid is permeated by a strong magnetic field $\vec{H} = \left(H_0\sqrt{1-\psi^2}\ ,0, H_0\psi\right)$ where $H_0 = |H|$ is the magnitude of the magnetic field and $\psi = \cos\theta$.

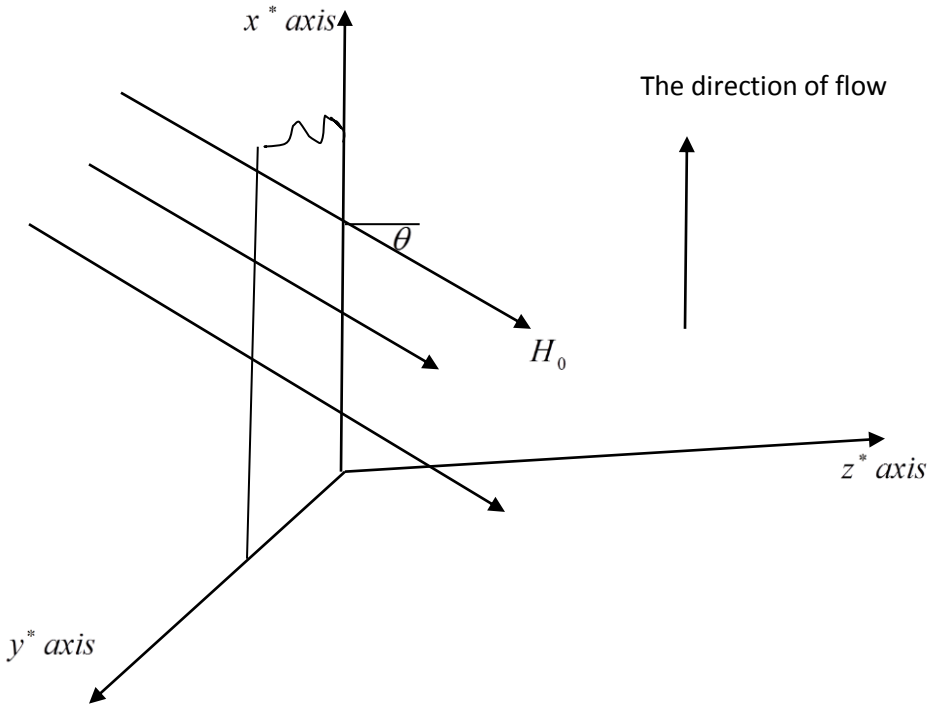

Figure 1: showing flow configuration

The continuity equation for the fluid flow under consideration is given by;

$$\frac{\partial w^*}{\partial z*} = 0 \qquad (1)$$

Since the fluids particle velocity equal to zero because of no-slip condition. On integration equation (3.4.9) gives the constant suction velocity

$$w^* = -w_0^* \qquad (2)$$

To determine the pressure gradient term in momentum equation

$\rho\left(\frac{\partial U_j}{\partial t} + U_j\frac{\partial U_i}{\partial x_j}\right) = -\frac{\partial p}{\partial x_j} + \rho\nu\nabla^2 U_i + \rho g + J\times B$ the momentum equation is evaluated at the edge of the boundary layer where $\rho \to \rho_\infty$ and $U \to 0$. The pressure term in the x^* direction, $-\frac{\partial p}{\partial x^*} = -\rho_\infty\, g$ results from the change in the elevation. The body force term in

Zain Publications
Company Registration No: UAN TS02E0015729
(Govt. of India, Ministry of Micro, Small & Medium Enterprises)
Contact Person: Dr. Mohd Zainuddin
Address: #12-1-898, North Lalaguda, Secunderabad, Telangana, India
IJRIT
Ngesa Joel Ochola, International Journal of Robotics and Information Technology, Volume 1, Issue 2, Dec 2017, Pg: 74-103

eqn. 2.7 along negative x^* direction is $-\rho g$. Combining the pressure term and the body force term gives.

$$-\rho g - \frac{\partial p}{\partial x*} = g(\rho_\infty - \rho) \tag{3}$$

If the volumetric coefficient of thermal expansion is defined by

$$\beta = -\frac{1}{\rho}\left(\frac{\Delta\rho}{\Delta T}\right)_p = -\frac{1}{\rho}\left(\frac{\rho_\infty^* - \rho^*}{T_\infty^* - T^*}\right) = \frac{1}{\rho}\left(\frac{\rho_\infty^* - \rho^*}{T^* - T_\infty^*}\right) \tag{4}$$

and the volumetric coefficient of thermal expansion with concentration of the fluid by

$$\beta' = -\frac{1}{\rho}\left(\frac{\Delta\rho}{\Delta C}\right)_p = -\frac{1}{\rho}\left(\frac{\rho_\infty^* - \rho^*}{C_\infty^* - C^*}\right) = \frac{1}{\rho}\left(\frac{\rho_\infty^* - \rho^*}{C^* - C_\infty^*}\right) \tag{5}$$

From equation (1) and equation (2) we have,

$$\begin{aligned} \beta\rho(T^* - T_\infty^*) &= p_\infty^* - p^* \\ \beta'\rho(C^* - C_\infty^*) &= p_\infty^* - p^* \end{aligned} \tag{6}$$

The total change in density as a result of temperature and concentration is given by

$$\Delta\rho = \beta\rho(T^* - T_\infty) + \beta'\rho(C^* - C_\infty^*) \tag{7}$$

From Ohm's law $J = \sigma(q \times B)$, where J is the electric current density $J = (J_{x^*}, J_{y^*}, J_{z^*})$ and B is the magnetic induction, $B = (\mu_e H)$ which in component form is given as,

$$B_{x^*} = \mu_e H_0 \sin\theta$$

$$B_{y^*} = 0$$

$$B_{z^*} = \mu_e H_0 \cos\theta$$

$$J = \sigma \begin{vmatrix} i & j & k \\ u^* & v^* & 0 \\ B_{x^*} & 0 & B_{z^*} \end{vmatrix} = \sigma\left(v^* B_{z^*} i - u^* B_{z^*} j\right) = \sigma\mu_e H_0 \psi (v^* i - u^* j) \tag{8}$$

Where the term in equation (2.7) can be simplified as,

$$J \times B = \begin{vmatrix} i & j & k \\ J_{x^*} & J_{y^*} & 0 \\ \mu_e H_0\sqrt{1-\psi^2} & 0 & \mu_e H_0 \psi \end{vmatrix} = iJ_{y*}\mu_e H_0 \psi - jJ_{x^*}\mu_e H_0 \tag{9}$$

From the equation of conservation of electric charges $\nabla \cdot J = 0$, gives $J_{z^*} = \text{constant}$, this constant is zero, since $J_{z^*} = 0$ at the plate which is electrically non- conducting hence $J_{z^*} = 0$ everywhere in the flow, $B_{y^*} = 0$ due to the geometrical nature of our problem.

Substituting equations (3.5.5) and (3.5.7) in equation (3.4.2) and writing the result in component

Zain Publications
Company Registration No: UAN TS02E0015729
(Govt. of India, Ministry of Micro, Small & Medium Enterprises)
Contact Person: Dr. Mohd Zainuddin
Address: #12-1-898, North Lalaguda, Secunderabad, Telangana, India
IJRIT
Ngesa Joel Ochola, International Journal of Robotics and Information Technology, Volume 1, Issue 2, Dec 2017, Pg: 74-103

form to obtain;

$$\rho\left(\frac{\partial u^*}{\partial t^*}+u^*\frac{\partial u^*}{\partial x^*}-w_0^*\frac{\partial u^*}{\partial z^*}\right)=\mu\left(\frac{\partial^2 u^*}{\partial x^{*2}}+\frac{\partial^2 u^*}{\partial z^{*2}}\right)+\beta\rho\left(T^*-T_\infty^*\right)+\beta'\rho\left(C^*-C_\infty^*\right)+\mu_e\psi H_0 J_{x^*} \tag{10}$$

$$\rho\left(\frac{\partial v^*}{\partial t^*}+u^*\frac{\partial v^*}{\partial x^*}-w_0^*\frac{\partial v^*}{\partial z^*}\right)=\mu\left(\frac{\partial^2 v^*}{\partial x^{*2}}+\frac{\partial^2 u^*}{\partial z^{*2}}\right)-\mu_e\psi H_0 J_{y^*} \tag{11}$$

The generalized ohm's law including the effect of Hall current is written as;

$$j+\frac{we\tau e}{H}\left(j\times H\right)=\delta\left[E+\mu_e\left(q\times H\right)+\frac{1}{e\eta_e}\nabla p_e\right] \tag{12}$$

For the partially ionized fluids the electron pressure gradient may be neglected.

In this case we consider a short circuit problem in which the applied electronic field =0. Thus neglecting electron pressure the x and y components become;

$$j+\frac{we\tau e}{H}\left(j\times H\right)=\delta\mu_e\left(q\times H\right) \tag{13}$$

Expanding the equation we get

$$\left(J_y\ ,J_z\right)+\frac{we\tau e}{H}\left(j_z H_0\ ,-j_y H_0\right)=\delta\mu_e\left(vH_0-w_0H_0\right) \tag{14}$$

Solving these equations for current density components j_y *and* j_z

$$J_y=\frac{\delta\mu_e H_0\left(mv-w\right)}{1+m^2} \tag{15}$$

$$J_z=-\frac{\delta\mu_e H_0\left(v-mw\right)}{1+m^2} \tag{16}$$

Where $m=we\tau$ is the hall parameter.

Substituting equations (3.48) and (3.49) in the momentum equations and introducing the shear stress terms $\frac{\partial uv}{\partial x}$ and $\frac{\partial uw}{\partial x}$ yields

$$\rho\left(\frac{\partial u^*}{\partial t^*}+u^*\frac{\partial u^*}{\partial x^*}-w_0^*\frac{\partial u^*}{\partial z^*}\right)=\mu\left(\frac{\partial^2 u^*}{\partial x^{*2}}+\frac{\partial^2 u^*}{\partial z^{*2}}\right)+\beta\rho\left(T^*-T_\infty^*\right)+\beta'\rho\left(C^*-C_\infty^*\right)-\frac{\partial uv}{\partial x}+\frac{\delta\psi\mu_e^2 H_0^2\left(mv-w\right)}{1+m^2} \tag{17}$$

$$\rho\left(\frac{\partial v^*}{\partial t^*}+u^*\frac{\partial v^*}{\partial x^*}-w_0^*\frac{\partial v^*}{\partial z^*}\right)=\mu\left(\frac{\partial^2 v^*}{\partial x^{*2}}+\frac{\partial^2 u^*}{\partial z^{*2}}\right)-\frac{\partial uw}{\partial x}-\frac{\delta\psi\mu_e^2 H_0^2\left(v-mw\right)}{1+m^2} \tag{18}$$

If electrical dissipation function and electromagnetic dissipation terms are neglected the energy equation becomes,

Zain Publications
Company Registration No: UAN TS02E0015729
(Govt. of India, Ministry of Micro, Small & Medium Enterprises)
Contact Person: Dr. Mohd Zainuddin
Address: #12-1-898, North Lalaguda, Secunderabad, Telangana, India
IJRIT
Ngesa Joel Ochola, International Journal of Robotics and Information Technology, Volume 1, Issue 2, Dec 2017, Pg: 74-103

$$\frac{\partial T^*}{\partial t^*}+u^*\frac{\partial T^*}{\partial x^*}-w_0^*\frac{\partial T^*}{\partial z^*}=\frac{k}{\rho c_p}\left(\frac{\partial^2 T}{\partial x^{*2}}+\frac{\partial^2 T}{\partial z^{*2}}\right)+\phi+\frac{Q^+}{\rho c_p} \tag{19}$$

Finally the concentration equation is given by,

$$\frac{\partial C^*}{\partial t^*}+u^*\frac{\partial C^*}{\partial x^*}-w_0^*\frac{\partial C^*}{\partial z^*}=D\left(\frac{\partial^2 C^*}{\partial x^{*2}}+\frac{\partial^2 C^*}{\partial z^{*2}}\right) \tag{20}$$

Turbulent flow is defined as an eddying motion in which the various quantities show random variation with time and space coordinates, so that statistically distinct average values can be discerned (Hinze 1974, Reynolds 1976). The basic nature of turbulence can be described as a wide spectrum of various sized vortex elements which interact with each other in a highly random and unsteady fashion. That is

$$\rho=\bar{\rho}+\rho', \qquad u_j=\bar{u}_j+u_j' \qquad , \; p=\bar{p}+p'$$

Thus the continuity equation reduces to

$$\frac{\partial\bar{\rho}}{\partial t}+\frac{\partial}{\partial x_j}\left(\overline{\rho u_j}\right)+\frac{\partial}{\partial x_j}\left(\overline{\rho' u_j'}\right)=0 \tag{21}$$

Averaging and adopting the adopting the Boussinessque approximation on the shear stress terms

$$\frac{\partial\left(\bar{u}^*\bar{v}^*\right)}{\partial x^*};\frac{\partial\left(\bar{u}^*\bar{w}^*\right)}{\partial x^*}$$

$$\tau=-\rho\bar{v}\bar{w}=A\frac{\partial\bar{v}}{\partial z} \tag{24}$$

From experiment Prandtl deduced that;

$$\rho\bar{v}\bar{w}=-\rho l^2\left(\frac{\partial\bar{v}}{\partial z}\right)^2 \tag{25}$$

Taking $l=kz$ where k is the Von Karman constant so we have;

$$\bar{u}^*\bar{v}^*=-k^2x^2\left(\frac{\partial\bar{v}^*}{\partial x^*}\right)^2 \tag{26}$$

$$\bar{u}^*\bar{w}^*=-k^2x^2\left(\frac{\partial\bar{w}^*}{\partial x^*}\right)^2 \tag{27}$$

Substituting in equations (17) and (18) we get

$$\begin{aligned}\frac{\partial\bar{u}^*}{\partial t^*}+\bar{u}^*\frac{\partial\bar{u}^*}{\partial x^*}-\bar{w}_0^*\frac{\partial\bar{u}^*}{\partial z^*}&=\frac{\mu}{\rho}\left(\frac{\partial^2\bar{u}^*}{\partial x^{*2}}+\frac{\partial^2\bar{u}^*}{\partial z^{*2}}\right)+\beta\left(T^*-T_\infty^*\right)\\&+\beta'\left(C^*-C_\infty^*\right)-\frac{\partial}{\partial x^*}\left[k^2x^2\left(\frac{\partial v^*}{\partial x^*}\right)^2\right]-\frac{\delta\psi\mu_e^2H_0^2\left(mv^*-w^*\right)}{\rho\left(1+m\right)^2}\end{aligned} \tag{28}$$

Zain Publications
Company Registration No: UAN TS02E0015729
(Govt. of India, Ministry of Micro, Small & Medium Enterprises)
Contact Person: Dr. Mohd Zainuddin
Address: #12-1-898, North Lalaguda, Secunderabad, Telangana, India
IJRIT
Ngesa Joel Ochola, International Journal of Robotics and Information Technology, Volume 1, Issue 2, Dec 2017, Pg: 74-103

$$\frac{\partial \bar{v}^*}{\partial t^*}+\bar{u}^*\frac{\partial \bar{v}^*}{\partial x^*}-\bar{w}_0^*\frac{\partial \bar{v}^*}{\partial z^*}=\frac{\mu}{\rho}\left(\frac{\partial^2 \bar{v}^*}{\partial x^{*2}}+\frac{\partial^2 \bar{u}^*}{\partial z^{*2}}\right)$$
$$-\frac{\partial}{\partial x^*}\left[k^2x^2\left(\frac{\partial \bar{w}^*}{\partial x^*}\right)^2\right]-\frac{\delta\psi\mu_e^2H_0^2\left(v^*-mw^*\right)}{\rho(1+m)^2} \quad (29)$$

It is assumed that the induced magnetic field is negligible so that the fluid is permeated by a strong field $\vec{H}=\left(H_0\sqrt{1-\psi^2}\ ,0,H_0\psi\right)$ where $H_0=|H|$ is the magnitude of the magnetic field and $\psi=\cos\theta$. This assumption hold for small magnetic Raynold's number. The equation of Electric charge $\nabla\cdot J=0$ gives $J_{z^*}=cons\tan t$; this constant is assumed to be zero, since $J_{z^*}=0$ at the plate, which is electrically non-conducting. It implies that $J_{z^*}=0$ everywhere in the flow. Taking into consideration the Hall current (due to electrons), Ion-slip current (due to ions) and collisions between electrons and neutral particles, we obtain a modified Ohm's law of the form,

$$J=\sigma\left[E+q\times B\right]-\frac{\omega_e\tau_e}{B_0}\left[J\times B\right]+\frac{\omega_e\tau_e\omega_i\tau_i}{B_0^2}(J\times B)\times B \quad (30)$$

For short circuit problem the applied electric field $E=0$. Equation (30) becomes

$$J=\sigma\left[q\times B\right]-\frac{\omega_e\tau_e}{B_0}\left[J\times B\right]+\frac{\omega_e\tau_e\omega_i\tau_i}{B_0^2}(J\times B)\times B \quad (31)$$

Solving (31) for J_{x^*} *and* J_{y^*} yields,

$$J_{x^*}=\frac{\sigma\mu_eH_0\psi\left[v^*(1+m_*n_*\psi^2)+u^*m_*\psi\right]}{\left[1+m_*n_*\psi^2\right]^2+m_*^2\psi^2} \quad (32)$$

$$J_{y^*}=\frac{\sigma\mu_eH_0\psi\left[v^*m_*\psi-u(1+m_*n_*\psi^2)\right]}{\left[1+m_*n_*\psi^2\right]^2+m_*^2\psi^2} \quad (33)$$

Where $m_*=\omega_e\tau_e$ (Hall parameter) and $n_*=\omega_i\tau_i$ (Ion-slip parameter).

Substituting equation (32) and (33) in equation (28) and (29) from equations we obtain,

$$\rho\left(\frac{\partial u^*}{\partial t^*}+u^*\frac{\partial u^*}{\partial x^*}-w_0^*\frac{\partial u^*}{\partial z^*}\right)=\mu\left(\frac{\partial^2 u^*}{\partial x^{*2}}+\frac{\partial^2 u^*}{\partial z^{*2}}\right)+\beta\rho\left(T^*-T_\infty^*\right)$$

$$+\beta'\rho\left(C^*-C_\infty^*\right)-\frac{\partial uv}{\partial x}+\frac{\sigma\mu_e^2H_0^2\psi^2\left[v^*m_*\psi-u^*(1+m_*n_*\psi^2)\right]}{\left[1+m_*n_*\psi^2\right]^2+m_*^2\psi^2} \quad (34)$$

Zain Publications
Company Registration No: UAN TS02E0015729
(Govt. of India, Ministry of Micro, Small & Medium Enterprises)
Contact Person: Dr. Mohd Zainuddin
Address: #12-1-898, North Lalaguda, Secunderabad, Telangana, India
IJRIT
Ngesa Joel Ochola, International Journal of Robotics and Information Technology, Volume 1, Issue 2, Dec 2017, Pg: 74-103

$$\rho\left(\frac{\partial v^*}{\partial t^*}+u^*\frac{\partial v^*}{\partial x^*}-w_0^*\frac{\partial v^*}{\partial z^*}\right)=\mu\left(\frac{\partial^2 v^*}{\partial x^{*2}}+\frac{\partial^2 v^*}{\partial z^{*2}}\right)-\frac{\partial uw}{\partial x}$$

$$-\frac{\sigma\mu_e^2 H_0^2\psi^2\left[v^* m_*\psi-u^*(1+m_* n_*\psi^2)\right]}{\left[1+m_* n_*\psi^2\right]^2+m_*^2\psi^2} \tag{35}$$

$$\frac{\partial T^*}{\partial t^*}+u^*\frac{\partial T^*}{\partial x^*}-w_0^*\frac{\partial T^*}{\partial z^*}=\frac{k}{\rho c_p}\left(\frac{\partial^2 T^*}{\partial x^{*2}}+\frac{\partial^2 T^*}{\partial z^{*2}}\right)+\frac{Q^+}{\rho c_p}$$

$$+\frac{\nu}{\rho c_p}\left[\left(\frac{\partial u^*}{\partial x^*}\right)^2+\left(\frac{\partial v^*}{\partial x^*}\right)^2+\left(\frac{\partial u^*}{\partial z^*}\right)^2+\left(\frac{\partial v^*}{\partial z^*}\right)^2\right] \tag{36}$$

And

$$\frac{\partial C^*}{\partial t^*}+u^*\frac{\partial C^*}{\partial x^*}-w_0^*\frac{\partial C^*}{\partial z^*}=D\left(\frac{\partial^2 C^*}{\partial x^{*2}}+\frac{\partial^2 C^*}{\partial z^{*2}}\right) \tag{37}$$

The following Non Dimensional numbers are used in this paper;

Raynold's number, Re

It is the ratio of inertia force to the viscous force acting on the fluid. If for any flow this number is less than one the inertia force is negligible and on the other hand if it is large, one can ignore viscous force and so the fluid can be taken as inviscid. It is given by

$$\mathrm{Re}=\frac{\rho UL}{\mu}=\frac{UL}{\nu}$$

It plays a role in forced convection; its role is the same as that of Grashof number in natural/free convection.

Its critical value governs the transition from laminar to turbulent in forced convection.

Prandtl number, Pr

It is the ratio of viscous force to thermal force acting on the fluid. It relates the velocity field with temperature field, and is the ratio of the transport properties ν *and* α, which govern the transport of momentum and energy respectively. It plays a role in heat transfer.

The Prandtl number is large when thermal conductivity is less than one and viscosity is large, and is small when viscosity is less than one and thermal conductivity is large.

Zain Publications
Company Registration No: UAN TS02E0015729
(Govt. of India, Ministry of Micro, Small & Medium Enterprises)
Contact Person: Dr. Mohd Zainuddin
Address: #12-1-898, North Lalaguda, Secunderabad, Telangana, India
IJRIT
Ngesa Joel Ochola, International Journal of Robotics and Information Technology, Volume 1, Issue 2, Dec 2017, Pg: 74-103

$$\Pr = \frac{\nu}{\alpha}; \quad \alpha = \frac{k}{\rho c} \quad ;$$

ν – *momentum* (*kinematic diffusivity*)

α – *thermal diffusivity*

Or $\Pr = \frac{\mu c_p}{k}$

Grashof number, Gr

This is another non-dimensional number, which usually occurs in natural convention problems. It is due to density differences resulting from concentration difference and not temperature differences and defined as the ratio of buoyancy forces to viscous forces acting on the fluid. Its critical value governs the transition from laminar to turbulent flow in natural/free convection.

The larger it is the stronger is the convective current.

$$Gr = \frac{\nu g \beta \left(T_w^* - T_\infty^*\right)}{U^3}$$

Eckert number, Ec

This is the ratio of the kinetic energy to thermal energy.

$$Ec = \frac{U^2}{c_p \left(T_w^* - T_\infty^*\right)}$$

Hartmann number, M

It is the ratio of magnetic force to the viscous force,

$$M^2 = \frac{\sigma \mu_e^2 H_0^2 \nu}{U\rho}$$

Schmidt number, Sc

This provides a measure of the relative effectiveness of momentum and mass transport by diffusion in the velocity field and concentration boundary layers respectively.

It relates the velocity field with the concentration field, and is the ratio of the transport properties ν *and* D, which govern the transport of momentum and mass respectively.

Plays a role in mass transfer; its role in mass transfer is the same as that of Prandtl number in heat transfer.

Zain Publications
Company Registration No: UAN TS02E0015729
(Govt. of India, Ministry of Micro, Small & Medium Enterprises)
Contact Person: Dr. Mohd Zainuddin
Address: #12-1-898, North Lalaguda, Secunderabad, Telangana, India
IJRIT
Ngesa Joel Ochola, International Journal of Robotics and Information Technology, Volume 1, Issue 2, Dec 2017, Pg: 74-103

$$Sc = \frac{\nu}{D}$$

ν – *momentum (kinematic) diffusivity*

D – *mass diffusivity*

Nusselt number, Nu

This parameter is equal to the dimensionless temperature gradient at the surface. It provides a measure of the convection heat transfer occurring at the surface.

$$Nu = \frac{\delta\theta}{\delta x}\Big|_{x=0}$$

Sherwood number, Sh

Is the dimensionless concentration gradient at the surface. It provides a measure of the convection mass transfer occurring at the surface.

$$Sh = \frac{\delta C}{\delta x}\Big|_{x=0}$$

In this study, all the variables with the superscript (*) star will represent dimensional variables and non-dimensionalization is based on the following sets of scaling variables.

On introducing the dimensionless quantities

$$t == \frac{t^* U^2}{\nu},\ x = \frac{x^* U}{\nu},\quad z = \frac{z^* U}{\nu},\ u = \frac{u*}{U},\quad v = \frac{v^*}{U},\ w_0 = \frac{w_0^*}{U},$$

$$\tau = \frac{\tau^*}{\rho U},\ \theta = \frac{T^* - T_\infty^*}{T_w^* - T_\infty^*},\ C = \frac{C^* - C_\infty^*}{C_w^* - C_\infty^*},\ Sc = \frac{D}{\nu},\ \delta = \frac{Q\nu}{kU^2},\quad (38)$$

$$Gr = \frac{\nu g\beta(T_w^* - T_\infty^*)}{U^3},\ Gc = \frac{\nu g\beta'(C_w^* - C_\infty^*)}{U^3}$$

Equations (34) to (37) becomes,

$$\frac{\partial u}{\partial t} + u\frac{\partial u}{\partial x} - w_0\frac{\partial u}{\partial z} = \left(\frac{\partial^2 u}{\partial x^2} + \frac{\partial^2 u}{\partial z^2}\right) + Gr\theta + GcC$$
$$-\left[2k^2 x\left(\frac{\partial v}{\partial x}\right)^2 + 2k^2 x^2\left(\frac{\partial^2 v}{\partial x^2}\right)\left(\frac{\partial v}{\partial x}\right)\right] + \frac{M^2\psi^2\left[\nu m_*\psi - u(1+m_* n_*\psi^2)\right]}{\left[1+m_* n_*\psi^2\right]^2 + m_*^2\psi^2} \quad (39)$$

$$\frac{\partial v}{\partial t} + u\frac{\partial v}{\partial x} - w_0\frac{\partial v}{\partial z} = \left(\frac{\partial^2 v}{\partial x^2} + \frac{\partial^2 v}{\partial z^2}\right) - \left[2k^2 x\left(\frac{\partial v}{\partial x}\right)^2 + 2k^2 x^2\left(\frac{\partial^2 v}{\partial x^2}\right)\left(\frac{\partial v}{\partial x}\right)\right]$$
$$-\frac{M^2\psi^2\left[um_*\psi + \nu(1+m_* n_*\psi^2)\right]}{\left[1+m_* n_*\psi^2\right]^2 + m_*^2\psi^2} \quad (40)$$

Zain Publications
Company Registration No: UAN TS02E0015729
(Govt. of India, Ministry of Micro, Small & Medium Enterprises)
Contact Person: Dr. Mohd Zainuddin
Address: #12-1-898, North Lalaguda, Secunderabad, Telangana, India
IJRIT
Ngesa Joel Ochola, International Journal of Robotics and Information Technology, Volume 1, Issue 2, Dec 2017, Pg: 74-103

$$\frac{\partial\theta}{\partial t}+u\frac{\partial\theta}{\partial x}-w_0\frac{\partial\theta}{\partial z}=\frac{1}{\Pr}\left[\frac{\partial^2\theta}{\partial x^2}+\frac{\partial^2\theta}{\partial z^2}\right]-\frac{\sigma}{\Pr}\theta+Ec\left[\left(\frac{\partial u}{\partial x}\right)^2+\left(\frac{\partial v}{\partial x}\right)^2+\left(\frac{\partial u}{\partial z}\right)^2+\left(\frac{\partial v}{\partial z}\right)^2\right] \quad (41)$$

and

$$\frac{\partial C}{\partial t}+u\frac{\partial C}{\partial x}-w_0\frac{\partial C}{\partial z}=\frac{1}{Sc}\left(\frac{\partial^2 C}{\partial x^2}+\frac{\partial^2 C}{\partial z^2}\right) \quad (42)$$

Initial and boundary conditions in non-dimensional form are,

For

$$\left.\begin{aligned} &t\le 0\ ,u(z,x,0)=0\,,v(z\,,x\,,0)=0\\ &\theta(z,\ \ x,\ 0)=0,\ C(z\ ,x,\ 0)=0\end{aligned}\right\} \quad (43)$$

For

$$\left.\begin{aligned} &t>0\ ,u(0,x,t)=1,v(0\,,x\,,t)=0\\ &\theta(0,\ \ x,\ t)=1,\ C(0\ ,x,\ t)=1\end{aligned}\right\} \quad (44)$$

For

$$\left.\begin{aligned} &t>0\ ,u(\infty,x,t)=0\,,v(\infty\,,x\,,t)=0\\ &\theta(\infty,\ \ x,\ t)=0,\ C(\infty\ ,x,\ t)=0\end{aligned}\right\} \quad (45)$$

Method of Solution

Equations (39) to (42) are highly non-linear and therefore exact solutions are not possible, in order to solve these equations a fast and stable method for the solution of finite difference approximation has been developed together with the initial and boundary condition (43) to (45). The profiles given by $u_{(k,i)}^{n+1}$, $v_{(k,i)}^{n+1}$, $\theta_{(k,i)}^{n+1}$ *and* $C_{(k,i)}^{n+1}$ are computed by the following algorithms,

$$u_{(k,i)}^{n+1}=\Delta t\left\{\begin{aligned} &-u_{(k,i)}^{n}\left[\frac{u_{(k,i+1)}^{n}-u_{(k,i-1)}^{n}}{2\Delta x}\right]+w_0\left[\frac{u_{(k+1,i)}^{n}-u_{(k-1.i)}^{n}}{2\Delta z}\right]+\frac{u_{(k+1,i)}^{n}-2u_{(k,i)}^{n}+u_{(k-1,i)}^{n}}{(\Delta z)^2}\\ &+\frac{u_{(k,i+1)}^{n}-2u_{(k,i)}^{n}+u_{(k,i-1)}^{n}}{(\Delta x)^2}+Gr\theta_{(k,i)}^{n}+GcC_{(k,i)}^{n}-2k^2i\Delta x\left(\frac{u_{(k,i+1)}^{n}-2u_{(k,i)}^{n}+u_{(k,i-1)}^{n}}{2\Delta x}\right)^2\\ &-2k^2(i\Delta x)^2\left(\frac{u_{(k,i+1)}^{n}-2u_{(k,i)}^{n}+u_{(k,i-1)}^{n}}{(\Delta x)^2}\right)^2\left(\frac{u_{(k,i+1)}^{n}-u_{(k,i)}^{n}}{2\Delta x}\right)\\ &-\frac{M^2\psi^2\left[v_{(k,i)}^{n}m_*\psi-u_{(k,i)}^{n}(1+m_*n_*\psi^2)\right]}{\left[1+m_*n_*\psi^2\right]^2+m_*^2\psi^2}\end{aligned}\right\}+u_{(k,i)}^{n} \quad (46)$$

Zain Publications
Company Registration No: UAN TS02E0015729
(Govt. of India, Ministry of Micro, Small & Medium Enterprises)
Contact Person: Dr. Mohd Zainuddin
Address: #12-1-898, North Lalaguda, Secunderabad, Telangana, India

$$v_{(k,i)}^{n+1} = \Delta t\left\{\begin{array}{l} -u_{(k,i)}^{n}\left[\dfrac{v_{(k,i+1)}^{n}-v_{(k,i-1)}^{n}}{2\Delta x}\right]+w_0\left[\dfrac{v_{(k+1,i)}^{n}-v_{(k-1.i)}^{n}}{2\Delta z}\right]+\dfrac{v_{(k+1,i)}^{n}-2v_{(k,i)}^{n}+v_{(k-1,i)}^{n}}{(\Delta z)^2} \\ +\dfrac{v_{(k,i+1)}^{n}-2v_{(k,i)}^{n}+v_{(k,i-1)}^{n}}{(\Delta x)^2}-2k^2 i\Delta x\left(\dfrac{u_{(k,i+1)}^{n}-2u_{(k,i)}^{n}+u_{(k,i-1)}^{n}}{2\Delta x}\right)^2 \\ -2k^2(i\Delta x)^2\left(\dfrac{u_{(k,i+1)}^{n}-2u_{(k,i)}^{n}+u_{(k,i-1)}^{n}}{(\Delta x)^2}\right)\left(\dfrac{u_{(k,i+1)}^{n}-u_{(k,i)}^{n}}{2\Delta x}\right) \\ -\dfrac{M^2\psi^2\left[u_{(k,i)}^{n}m_*\psi+v_{(k,i)}^{n}(1+m_*n_*\psi^2)\right]}{\left[1+m_*n_*\psi^2\right]^2+m_*^2\psi^2} \end{array}\right\}+u_{(k,i)}^{n} \tag{47}$$

$$\frac{\theta_{(k,i)}^{n+1}-\theta_{(k,i)}^{n}}{\Delta t}+u_{(k,i)}^{n}\left[\frac{\theta_{(k,i+1)}^{n}-\theta_{(k,i-1)}^{n}}{2\Delta x}\right]-w_0\frac{\theta_{(k+1,i)}^{n}-\theta_{(k-1,i)}^{n}}{2\Delta z}=\frac{1}{\Pr}\left[\frac{\theta_{(k,i+1)}^{n}-2\theta_{(k,i)}^{n}+\theta_{(k,i-1)}^{n}}{(\Delta x)^2}\right]$$

$$+\frac{1}{\Pr}\left[\frac{\theta_{(k+1,i)}^{n}-2\theta_{(k,i)}^{n}+\theta_{(k-1,i)}^{n}}{(\Delta z)^2}\right]-\frac{\sigma}{\Pr}\theta_{(k,i)}^{n}+Ec\left[\begin{array}{l}\left(\dfrac{u_{(k,i+1)}^{n}-u_{(k,i-1)}^{n}}{2\Delta x}\right)^2+\left(\dfrac{v_{(k,i+1)}^{n}-v_{(k,i-1)}^{n}}{2\Delta x}\right)^2 \\ +\left(\dfrac{u_{(k+1,i)}^{n}-u_{(k-1,i)}^{n}}{2\Delta z}\right)^2+\left(\dfrac{v_{(k+1,i)}^{n}-v_{(k-1,i)}^{n}}{2\Delta z}\right)^2\end{array}\right]+\theta_{(k,i)}^{n} \tag{48}$$

$$\theta_{(k,i)}^{n+1} = \Delta t\left\{\begin{array}{l} -u_{(k,i)}^{n}\left[\dfrac{\theta_{(k,i+1)}^{n}-\theta_{(k,i-1)}^{n}}{2\Delta x}\right]+w_0\left[\dfrac{\theta_{(k+1,i)}^{n}-\theta_{(k-1.i)}^{n}}{2\Delta z}\right]+\dfrac{1}{\Pr}\dfrac{\theta_{(k+1,i)}^{n}-2\theta_{(k,i)}^{n}+\theta_{(k-1,i)}^{n}}{(\Delta z)^2} \\ +\dfrac{1}{\Pr}\dfrac{\theta_{(k,i+1)}^{n}-2\theta_{(k,i)}^{n}+\theta_{(k,i-1)}^{n}}{(\Delta x)^2}-\dfrac{\sigma}{\Pr}\theta_{(k,i)}^{n}+Ec\left[\begin{array}{l}\left(\dfrac{u_{(k,i+1)}^{n}-u_{(k,i-1)}^{n}}{2\Delta x}\right)^2+\left(\dfrac{v_{(k,i+1)}^{n}-v_{(k,i-1)}^{n}}{2\Delta x}\right)^2 \\ +\left(\dfrac{u_{(k+1,i)}^{n}-u_{(k-1,i)}^{n}}{2\Delta z}\right)^2+\left(\dfrac{v_{(k+1,i)}^{n}-v_{(k-1,i)}^{n}}{2\Delta z}\right)^2\end{array}\right] \end{array}\right\}+\theta_{(k,i)}^{n} \tag{49}$$

And

Zain Publications
Company Registration No: UAN TS02E0015729
(Govt. of India, Ministry of Micro, Small & Medium Enterprises)
Contact Person: Dr. Mohd Zainuddin
Address: #12-1-898, North Lalaguda, Secunderabad, Telangana, India
IJRIT
Ngesa Joel Ochola, International Journal of Robotics and Information Technology, Volume 1, Issue 2, Dec 2017, Pg: 74-103

$$C_{(k,i)}^{n+1} = \Delta t\left\{-u_{(k,i)}^{n}\left[\frac{C_{(k,i+1)}^{n} - C_{(k,i-1)}^{n}}{2\Delta x}\right] + w_0\left[\frac{C_{(k+1,i)}^{n} - C_{(k-1.i)}^{n}}{2\Delta z}\right] + \frac{1}{Sc}\left[\left(\frac{C_{(k,i+1)}^{n} - 2C_{(k,i)}^{n} + C_{(k,i-1)}^{n}}{2\Delta x}\right) + \left(\frac{C_{(k+1,i)}^{n} - 2C_{(k,i)}^{n} + C_{(k-1,i)}^{n}}{2\Delta z}\right)^2\right]\right\} + C_{(k,i)}^{n} \quad (50)$$

5.13 Discussion of results

A program was written and run for various values of velocities, temperatures and concentration for the finite differences equations (34) to (37) using different values of the parameters $Sc, m, n, \sigma, wo, t, Gc, Ec \text{ and } \psi$. The velocities are classified as primary velocities (u) and secondary velocities (v) along the x and y axes respectively.

The concentration, velocity and temperature profiles are presented graphically in figures. Grashof number $Gr > 0, (+0.4)$ corresponding to cooling of the plate by free convection currents and Grashof number $Gr < 0, (-0.4)$ corresponds to heating of the plate by free convection currents. The magnetic parameter $M^2 = 5.0$ signifies a strong magnetic field and Prandtl number $\Pr = 0.71$ corresponds to air.

5.13.1 Figures and tables for $\Pr = 0.71, M^2 = 5.0, Gr = +0.4$;with ion-slip

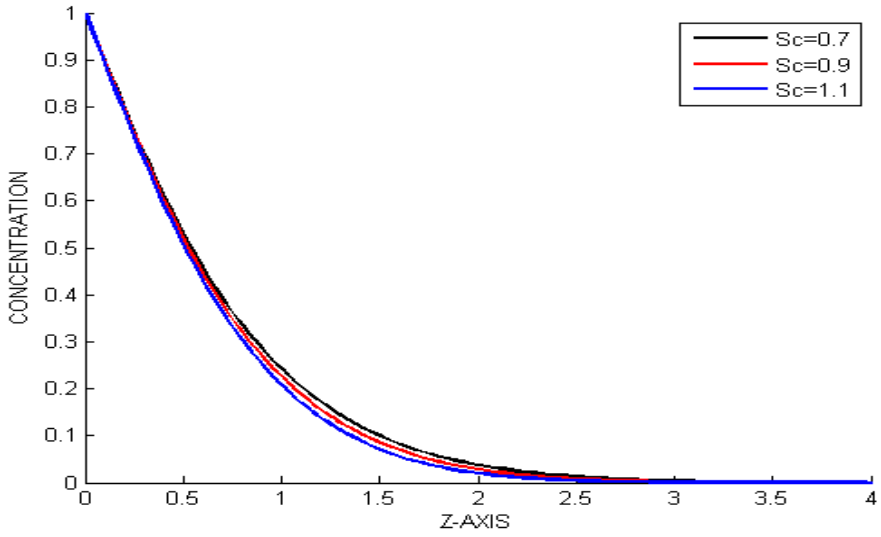

Figure 6.3a:Variation of concentration with Schmidt number Sc, with ion-slip

Zain Publications
Company Registration No: UAN TS02E0015729
(Govt. of India, Ministry of Micro, Small & Medium Enterprises)
Contact Person: Dr. Mohd Zainuddin
Address: #12-1-898, North Lalaguda, Secunderabad, Telangana, India
Ngesa Joel Ochola, International Journal of Robotics and Information Technology, Volume 1, Issue 2, Dec 2017, Pg: 74-103

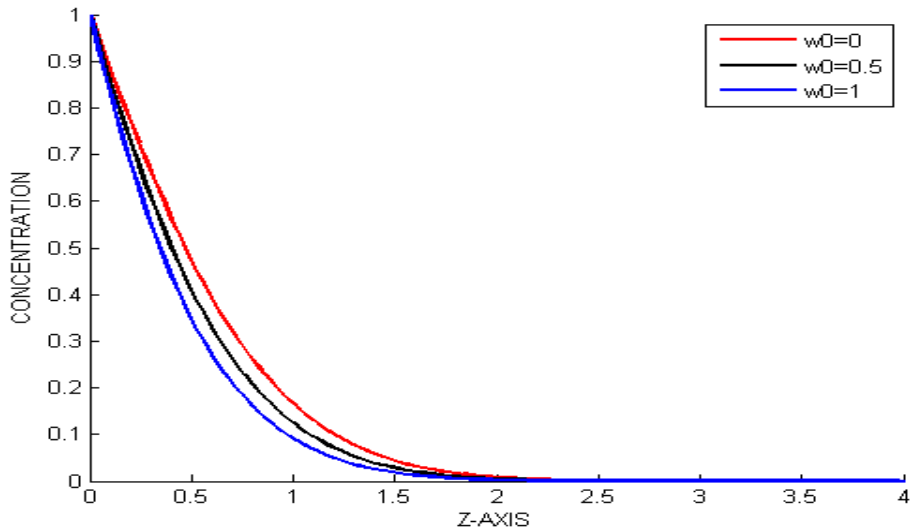

Figure 6.3b: Variation of concentration with Suction velocity *wo* , with ion-slip

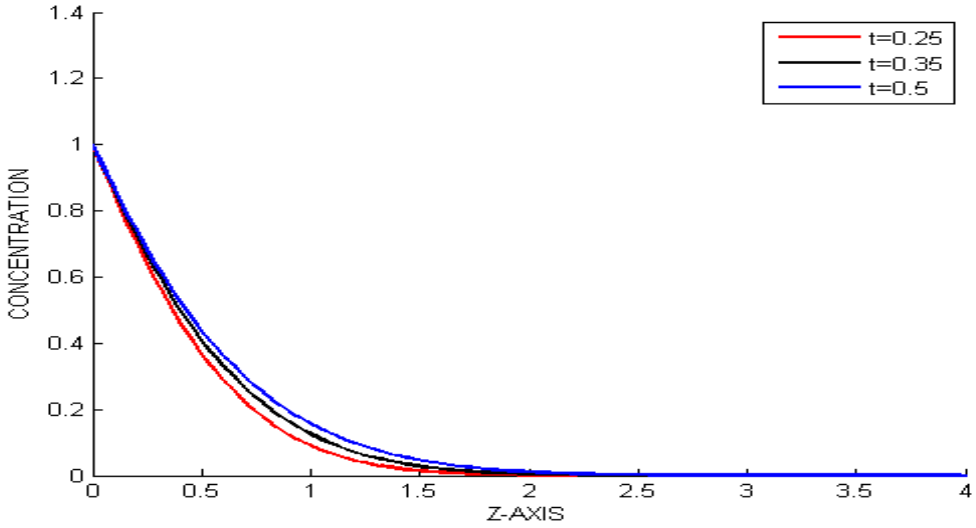

Figure 6.3c: Variation of concentration with time t, with ion-slip

From figure 6.3a - 6.3c; $Gr > 0, (+0.4)$, with ion-slip (n); we note that;

i.) An increase in mass diffusion parameter Sc causes a decrease in the concentration profiles (figure 6.3a)

ii.) Removal of suction velocity *wo* leads to an increase in the concentration profiles. This is due to the fact that this increases the growth of the boundary layers and hence the increase in the concentration profiles (figure 6.3b)

iii.) Increase in time increases the concentration profiles. With time the flow gets to the free stream and therefore its concentration increases (figure 6.3c)

Zain Publications
Company Registration No: UAN TS02E0015729
(Govt. of India, Ministry of Micro, Small & Medium Enterprises)
Contact Person: Dr. Mohd Zainuddin
Address: #12-1-898, North Lalaguda, Secunderabad, Telangana, India
Ngesa Joel Ochola, International Journal of Robotics and Information Technology, Volume 1, Issue 2, Dec 2017, Pg: 74-103

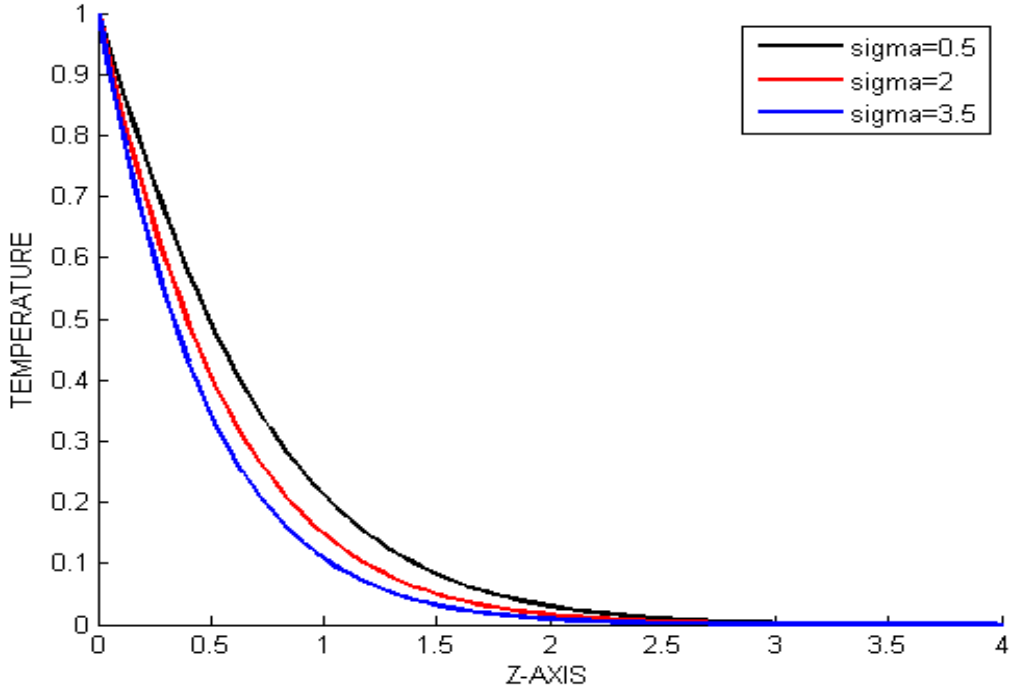

Figure 6.4a: Variation of Temperature with heat source parameter σ, with ion-slip

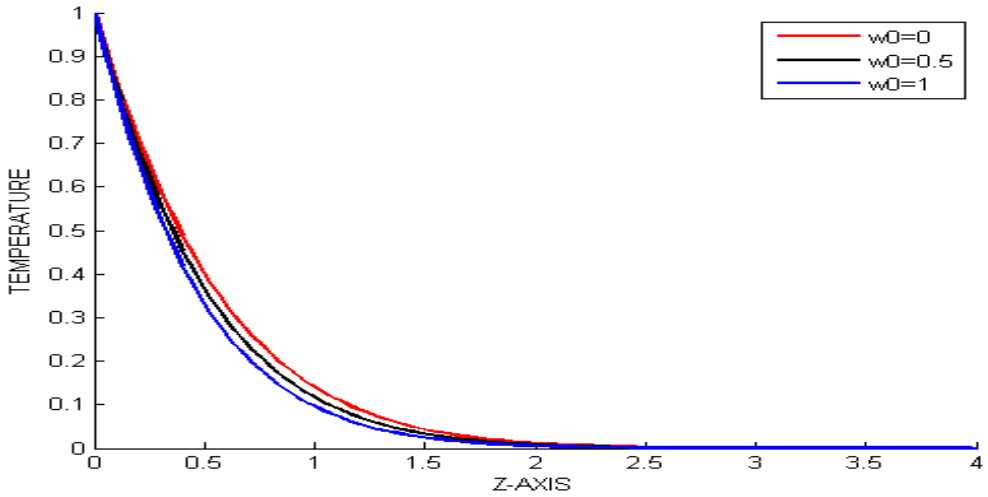

Figure 6.4b: Variation of Temperature with suction velocity *wo*, with ion-slip

Zain Publications
Company Registration No: UAN TS02E0015729
(Govt. of India, Ministry of Micro, Small & Medium Enterprises)
Contact Person: Dr. Mohd Zainuddin
Address: #12-1-898, North Lalaguda, Secunderabad, Telangana, India
IJRIT
Ngesa Joel Ochola, International Journal of Robotics and Information Technology, Volume 1, Issue 2, Dec 2017, Pg: 74-103

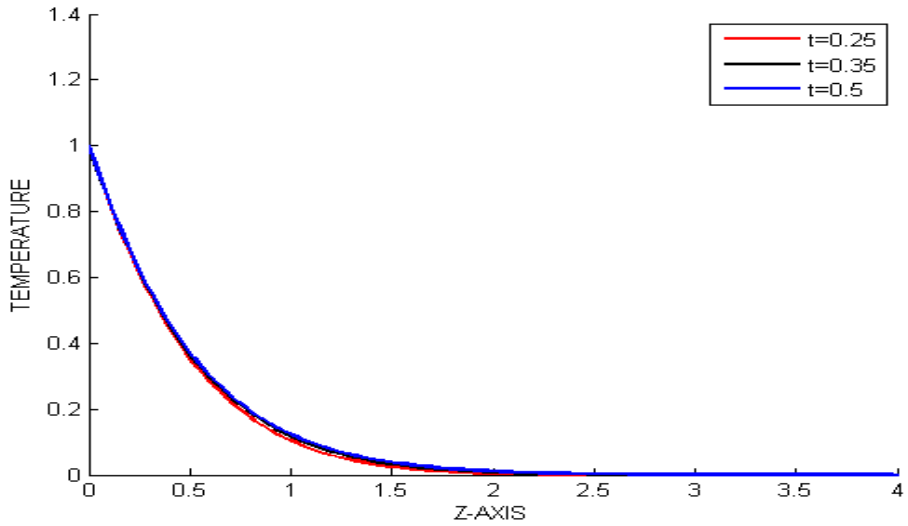

Figure 6.4c: Variation of Temperature with time t, with ion-slip

From figure 6.4a-6.4c; $Gr > 0, (+0.4)$, with ion-slip (n); we note that;

i.) An increase in time t or a decrease in heat source parameter σ leads to an increase in temperature profiles

ii.) Removal of suction velocity wo causes increase in temperature profiles.

ii.) Angle of inclination ψ causes no effect in temperature profiles

iii.) An increase in ion-slip parameter n causes no effect in temperature profiles

iv.) An increase in Hall parameter m leads to no effect in temperature profiles

v.) An increase in mass diffusion parameter Sc causes no effect in temperature profiles.

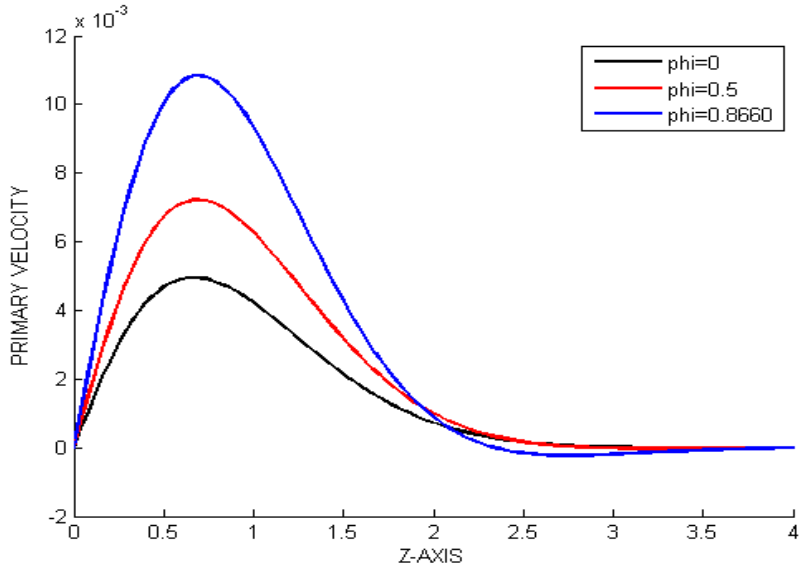

Figure 6.5 a: Variation of Primary velocity with angle of inclination ψ, with ion-slip

Zain Publications
Company Registration No: UAN TS02E0015729
(Govt. of India, Ministry of Micro, Small & Medium Enterprises)
Contact Person: Dr. Mohd Zainuddin
Address: #12-1-898, North Lalaguda, Secunderabad, Telangana, India
Ngesa Joel Ochola, International Journal of Robotics and Information Technology, Volume 1, Issue 2, Dec 2017, Pg: 74-103

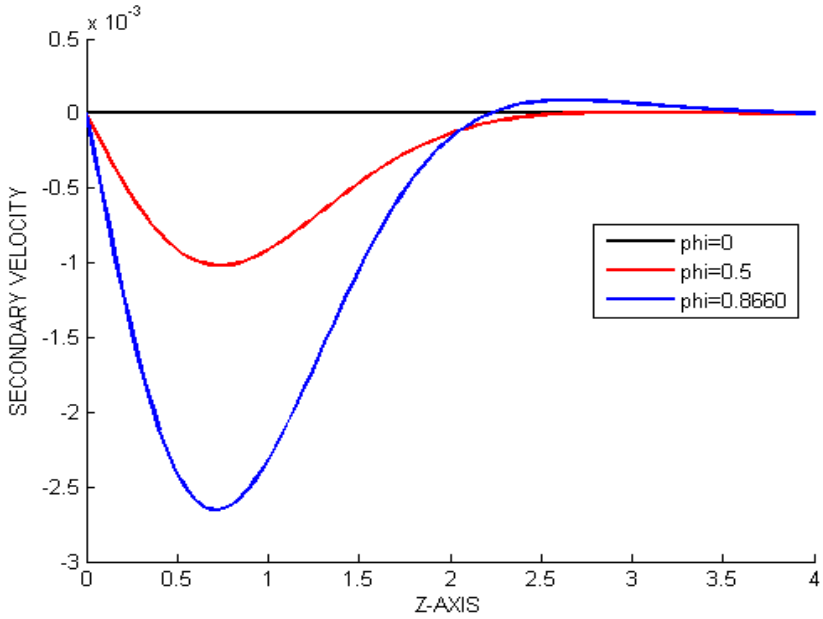

Figure 6.5 b: Variation of Secondary velocity with angle of inclination ψ, with ion-slip

From figure 6.5 a and 6.5 b; $Gr > 0, (+0.4)$ with ion-slip (n); we note that;

An increase in the angle of inclination ψ causes an increase in primary velocity profiles and a decrease in secondary profiles near the plate but away from the plate it decreases primary velocity but increase in secondary velocity to a point where both remain uniformly distributed.

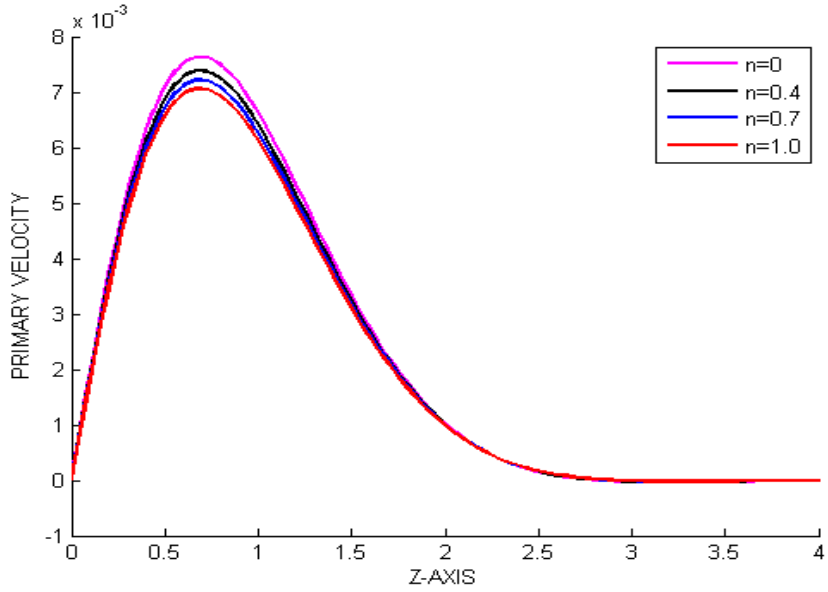

Figure 6.6 a: Variation of Primary velocity with ion-slip n

Zain Publications
Company Registration No: UAN TS02E0015729
(Govt. of India, Ministry of Micro, Small & Medium Enterprises)
Contact Person: Dr. Mohd Zainuddin
Address: #12-1-898, North Lalaguda, Secunderabad, Telangana, India
Ngesa Joel Ochola, International Journal of Robotics and Information Technology, Volume 1, Issue 2, Dec 2017, Pg: 74-103

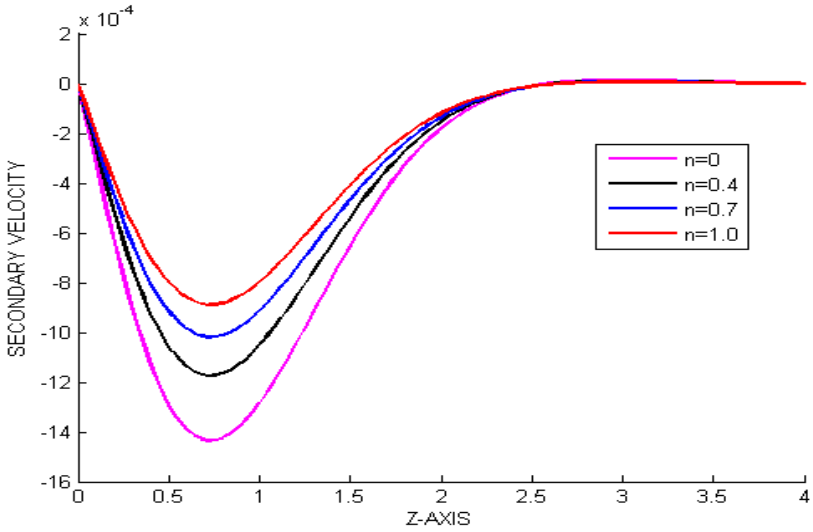

Figure 6.6 b: Variation of Secondary velocity with ion-slip n

From figure 6.6 a and 6.6 b; $Gr > 0, (+0.4)$ with ion-slip (n); we note that;

An increase in ion-slip parameter n leads to a negligible increase in primary velocity profiles but a decrease in secondary velocity profiles near the plate and remain constantly distributed away from the plate, this is because increase in ion-slip currents cause the force in the direction of the fluid flow to decrease leading to a decrease in the secondary velocity of the fluid. Since the magnitude of secondary velocity profile is very small, there is a very small increase in primary velocity profile with the change in the ion-slip currents.

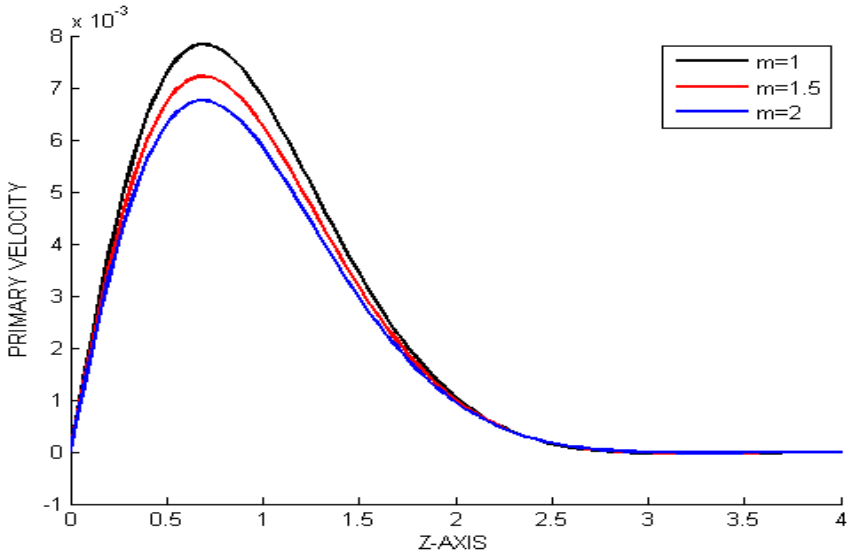

Figure 6.7 a: Variation of Primary velocity with Hall parameter m , with ion-slip:

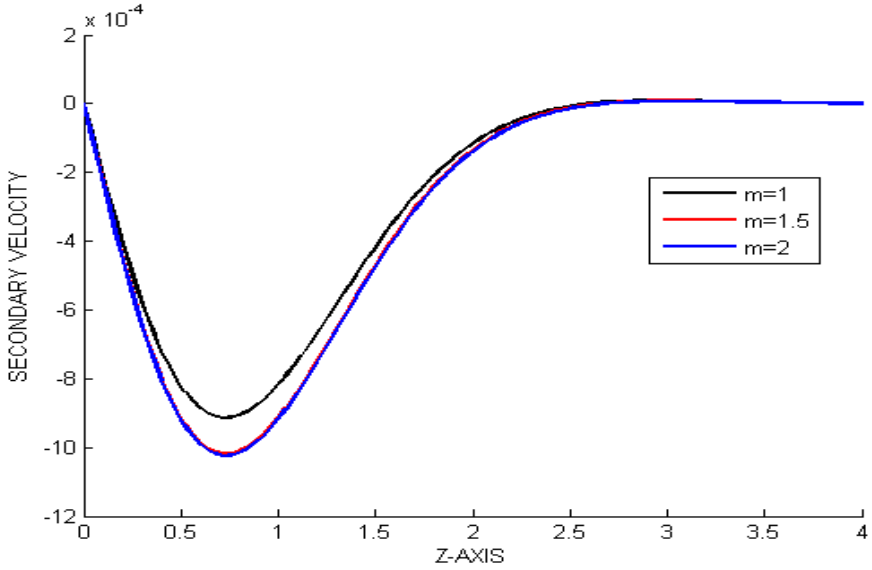

Figure 6.7 b: Variation of Secondary velocity with Hall parameter m, with ion-slip:

From figure 6.7 a and 6.7 b; $Gr > 0, (+0.4)$ with ion-slip (n); we note that;

An increase in Hall current parameter m causes a decrease in both primary and secondary velocity profiles.

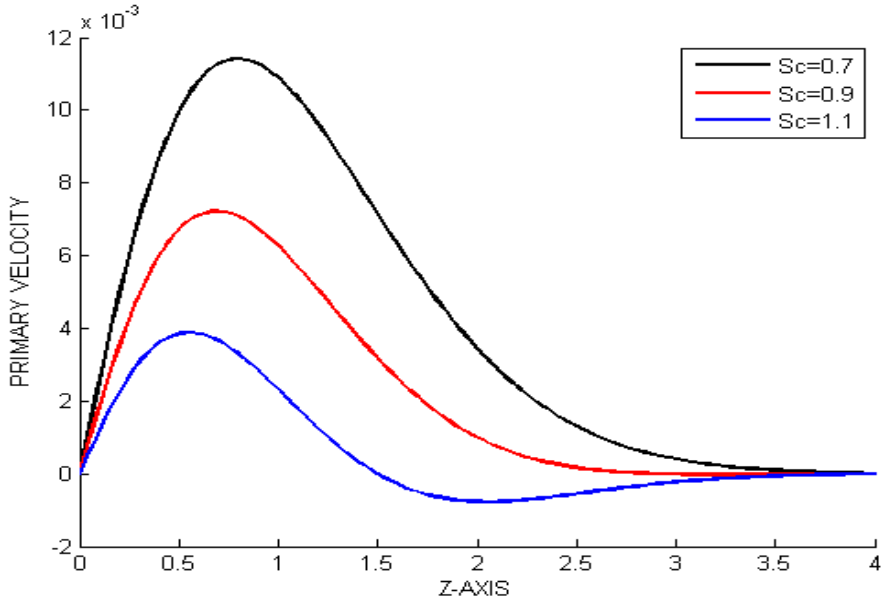

Figure 6.8 a: Variation of Primary velocity with Schmidt number Sc, with ion-slip

Zain Publications
Company Registration No: UAN TS02E0015729
(Govt. of India, Ministry of Micro, Small & Medium Enterprises)
Contact Person: Dr. Mohd Zainuddin
Address: #12-1-898, North Lalaguda, Secunderabad, Telangana, India
Ngesa Joel Ochola, International Journal of Robotics and Information Technology, Volume 1, Issue 2, Dec 2017, Pg: 74-103

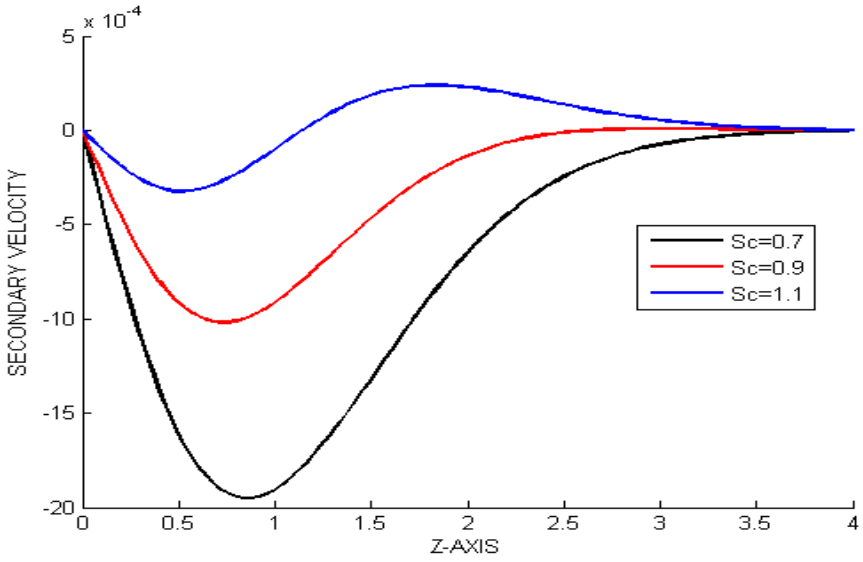

Figure 6.8 b: Variation of Secondary velocity with Schmidt number Sc, with ion-slip

From figure 6.8 a and 6.8 b; $Gr > 0, (+0.4)$ with ion-slip (n); we note that;

An increase in mass diffusion parameter Sc leads to a decrease in primary velocity profiles but an increase in secondary velocity profiles near the plate and the velocity profiles remain constantly distributed far away from the plate.

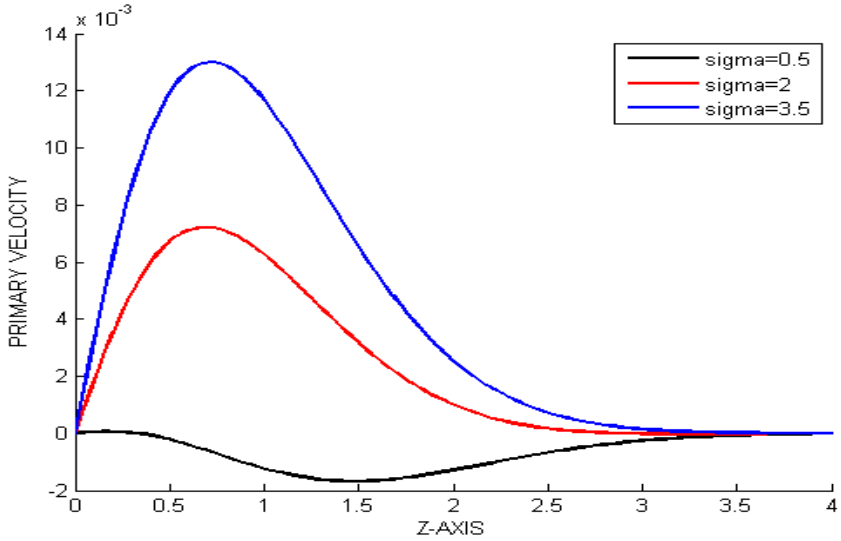

Figure 6.9 a: Variation of Primary velocity with heat source parameter σ, with ion-slip

Zain Publications
Company Registration No: UAN TS02E0015729
(Govt. of India, Ministry of Micro, Small & Medium Enterprises)
Contact Person: Dr. Mohd Zainuddin
Address: #12-1-898, North Lalaguda, Secunderabad, Telangana, India
Ngesa Joel Ochola, International Journal of Robotics and Information Technology, Volume 1, Issue 2, Dec 2017, Pg: 74-103

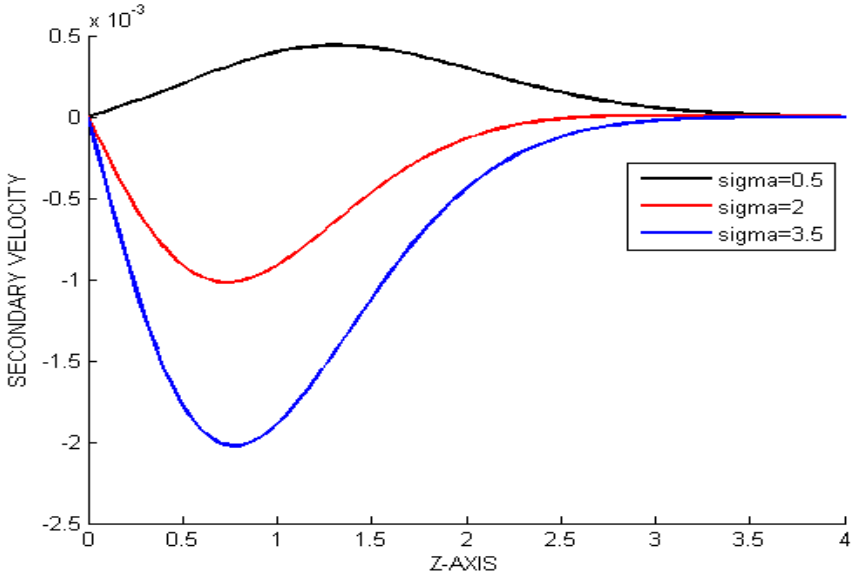

Figure 6.9 b: Variation of Secondary velocity with heat source parameter σ, with ion-slip

From figure 6.5 a and 6.5 b; $Gr > 0, (+0.4)$ with ion-slip (n); we note that;

An increase in heat source parameter σ leads to a decrease in primary velocity profiles but an increase in secondary velocity profiles near the plate and thereafter remain constantly distributed far away from the plate .

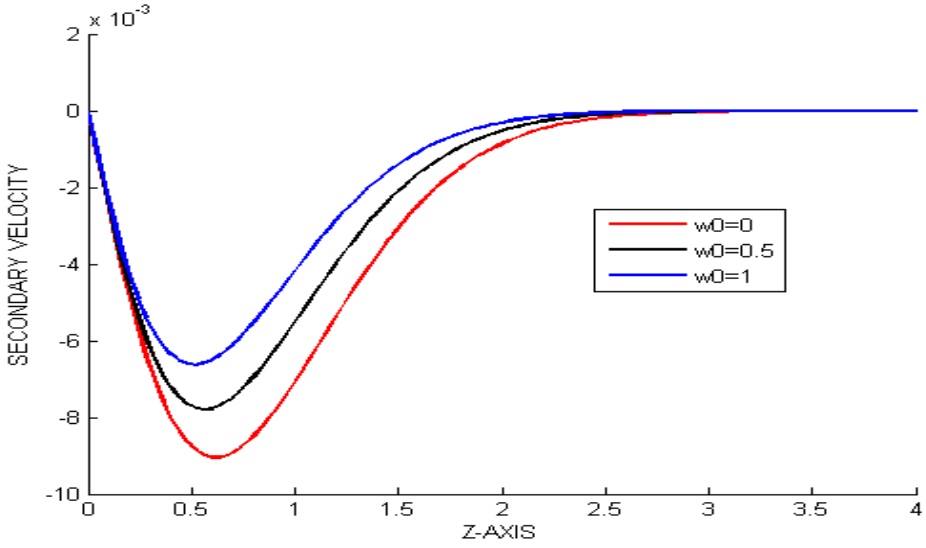

Figure 7.0a: Variation of Secondary velocity with suction velocity *wo*, with ion-slip

Zain Publications
Company Registration No: UAN TS02E0015729
(Govt. of India, Ministry of Micro, Small & Medium Enterprises)
Contact Person: Dr. Mohd Zainuddin
Address: #12-1-898, North Lalaguda, Secunderabad, Telangana, India
Ngesa Joel Ochola, International Journal of Robotics and Information Technology, Volume 1, Issue 2, Dec 2017, Pg: 74-103

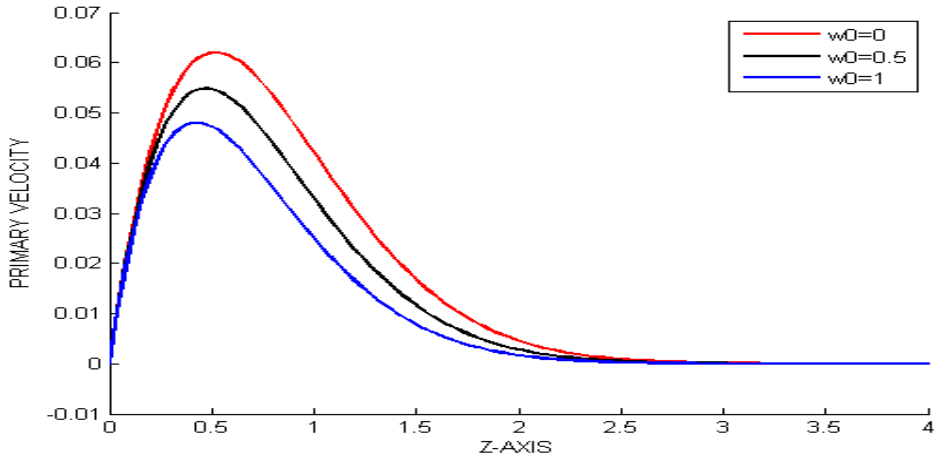

Figure 7.0b: Variation of Primary velocity with suction velocity *wo* , with ion-slip

From the figures 7.0a and 7.0b,we observe that;

i.) Removal of suction velocity *wo* leads to a gradual increase in primary velocity profiles near the plate to a maximum point after which the primary velocity profiles begin decrease uniformly then remain constantly distributed far away from the plate in the free stream (figure 7.0b)

ii.) Removal of suction velocity *wo* leads to a gradual decrease in secondary velocity profiles near the plate to a maximum after which the secondary velocity profiles begin to increase gradually then remain constantly distributed far away from the plate in the free streams (Figure 7.0a)

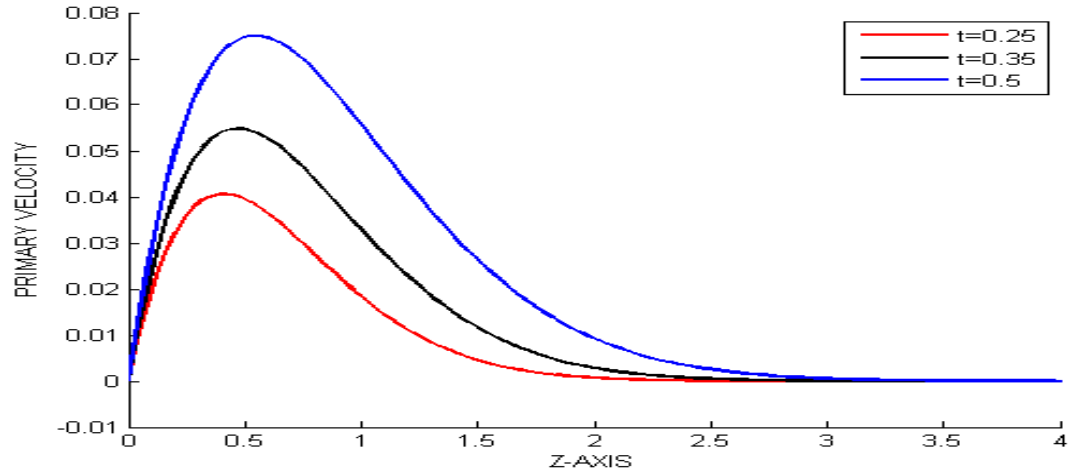

Figure 7.1a: Variation of Primary velocity with time *t* , with ion-slip

Zain Publications
Company Registration No: UAN TS02E0015729
(Govt. of India, Ministry of Micro, Small & Medium Enterprises)
Contact Person: Dr. Mohd Zainuddin
Address: #12-1-898, North Lalaguda, Secunderabad, Telangana, India
IJRIT
Ngesa Joel Ochola, International Journal of Robotics and Information Technology, Volume 1, Issue 2, Dec 2017, Pg: 74-103

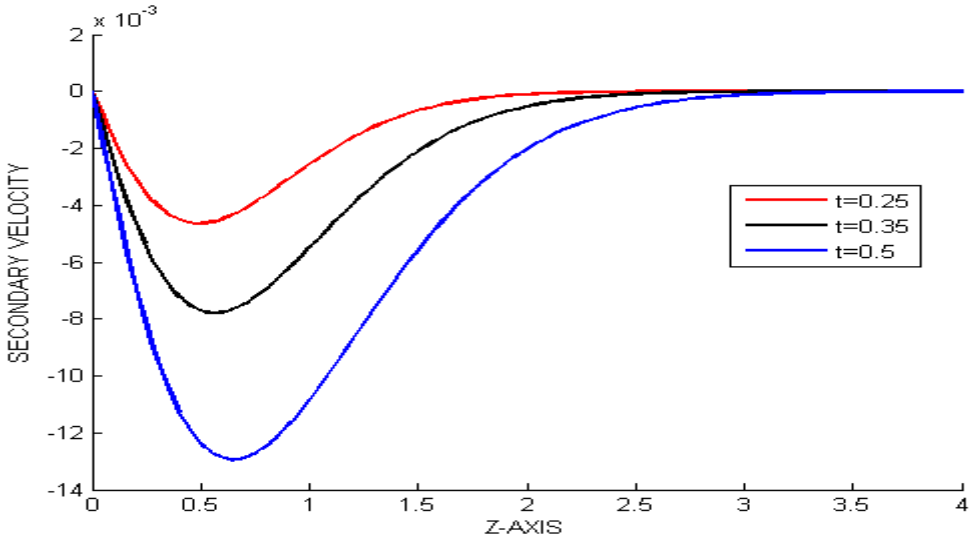

Figure 7.1b: Variation of Secondary velocity with time t, with ion-slip

From the figures 7.1a and 7.1b,we observe that;

i.) An increase in time t increases the primary velocity profiles. With time the flow gets to the free stream and therefore its velocity increases(figure 7.1a)

ii.) An increase in time t decreases the secondary velocity profiles. With time the flow gets to the free stream where the secondary velocity diminishes and therefore decrease in velocity profiles(figure 7.1b)

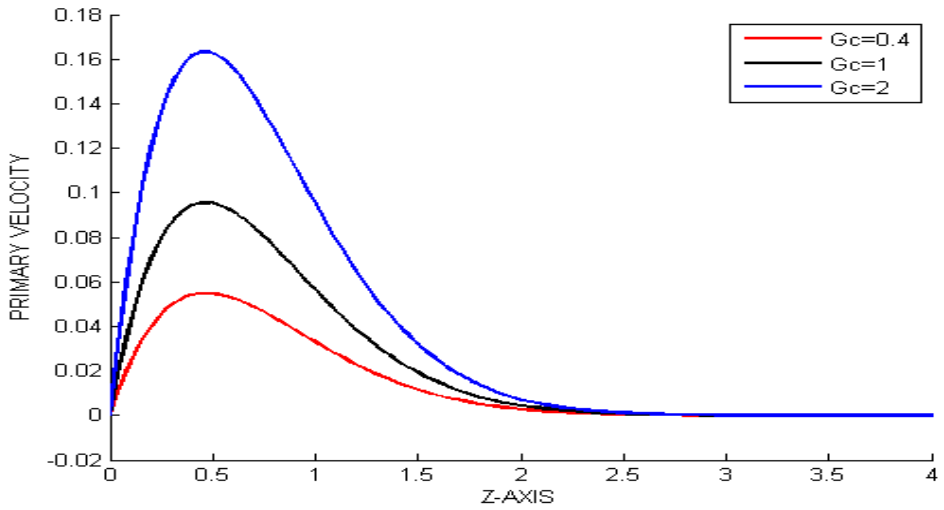

Figure 7.2a: Variation of Primary velocity with Modified Grashof Gc, with ion-slip

Zain Publications
Company Registration No: UAN TS02E0015729
(Govt. of India, Ministry of Micro, Small & Medium Enterprises)
Contact Person: Dr. Mohd Zainuddin
Address: #12-1-898, North Lalaguda, Secunderabad, Telangana, India
IJRIT
Ngesa Joel Ochola, International Journal of Robotics and Information Technology, Volume 1, Issue 2, Dec 2017, Pg: 74-103

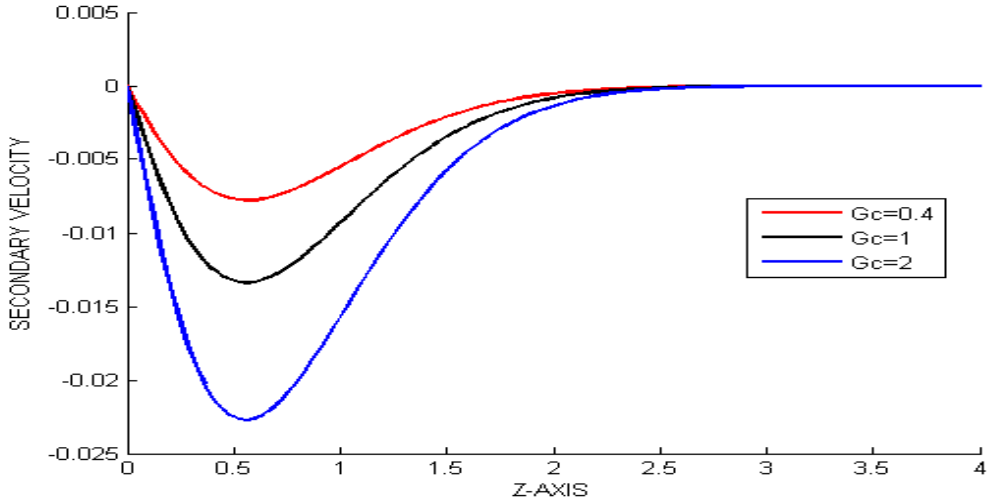

Figure 7.2b: Variation of Secondary velocity with Modified Grashof Gc, with ion-slip

From the figures 7.1a and 7.1b,we observe that;

i.) An increase in the Modified Grashof parameter Gc leads to a gradual increase in primary velocity profiles near the plate to a maximum after which the profiles begin to decrease gradually to a point in the free stream where the distribution remain constant and parallel to the z axis.

ii.) An increase in the Modified Grashof parameter Gc leads to a gradual decrease in secondary velocity profiles near the plate to a minimum after which the profiles begin to increase gradually to a point in the free stream where the distribution remain constant and parallel to the z axis.

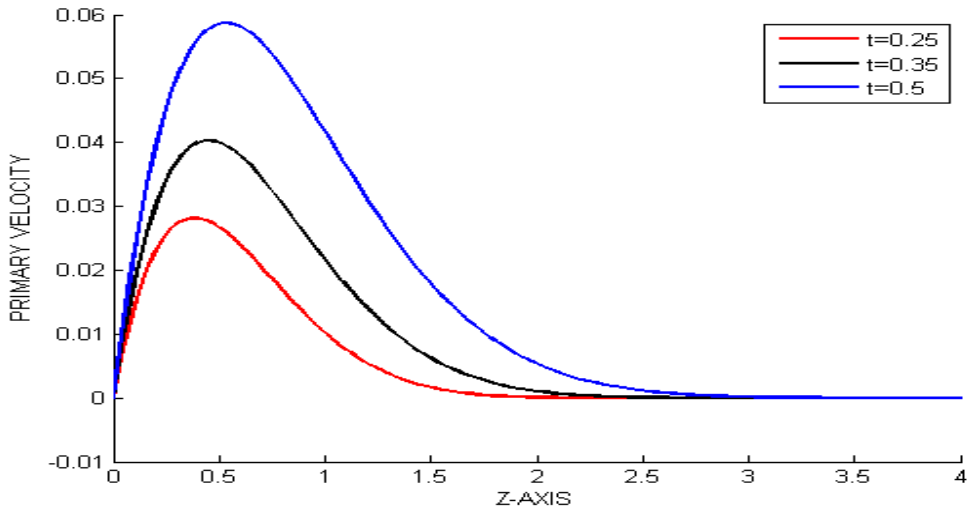

Figure 7.3a: Variation of Primary velocity with time $t, Gr = -0.4$, with ion-slip

Zain Publications
Company Registration No: UAN TS02E0015729
(Govt. of India, Ministry of Micro, Small & Medium Enterprises)
Contact Person: Dr. Mohd Zainuddin
Address: #12-1-898, North Lalaguda, Secunderabad, Telangana, India
Ngesa Joel Ochola, International Journal of Robotics and Information Technology, Volume 1, Issue 2, Dec 2017, Pg: 74-103

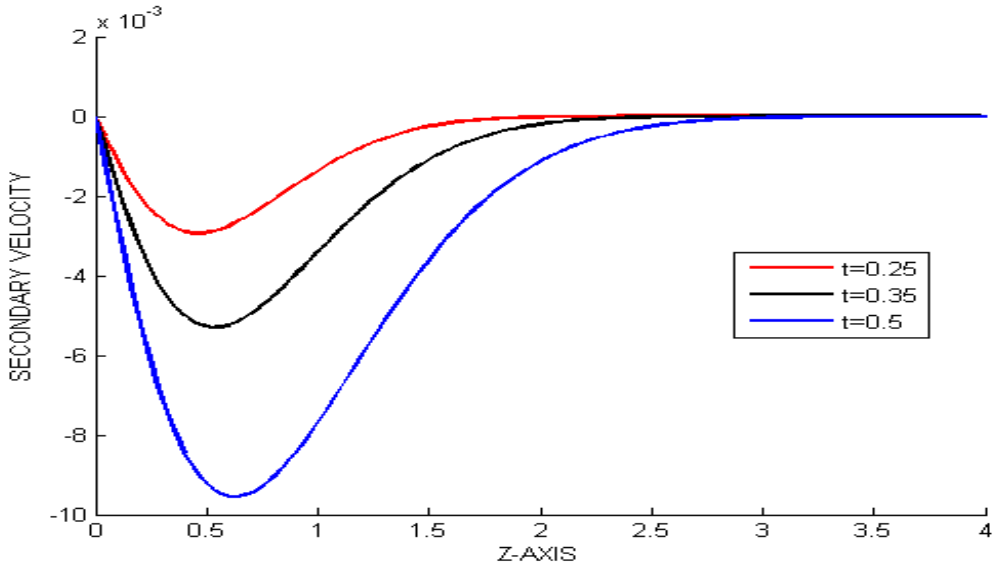

Figure 7.3b: Variation of Secondary velocity with time $t, Gr = -0.4$, with ion-slip

From figures 7.3a to 7.3b,we observe that;
An increase in time t leads to an increase in primary velocity profiles but a decrease in secondary velocity profiles from the curves $t = 0.25$ *to* $t = 0.5$ *and* $t = 0.5$ *to* 0.25 respectively near the plate and the velocity remain constanly distributed far away from the plate.

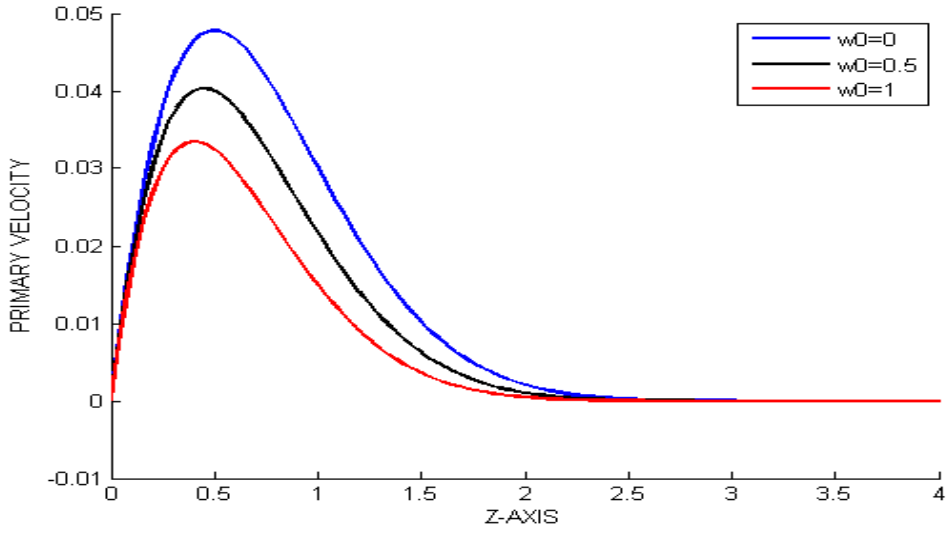

Figure 7.4a: Variation of Primary velocity with Suction velocity $wo, Gr = -0.4$, with ion-slip

Zain Publications
Company Registration No: UAN TS02E0015729
(Govt. of India, Ministry of Micro, Small & Medium Enterprises)
Contact Person: Dr. Mohd Zainuddin
Address: #12-1-898, North Lalaguda, Secunderabad, Telangana, India
IJRIT
Ngesa Joel Ochola, International Journal of Robotics and Information Technology, Volume 1, Issue 2, Dec 2017, Pg: 74-103

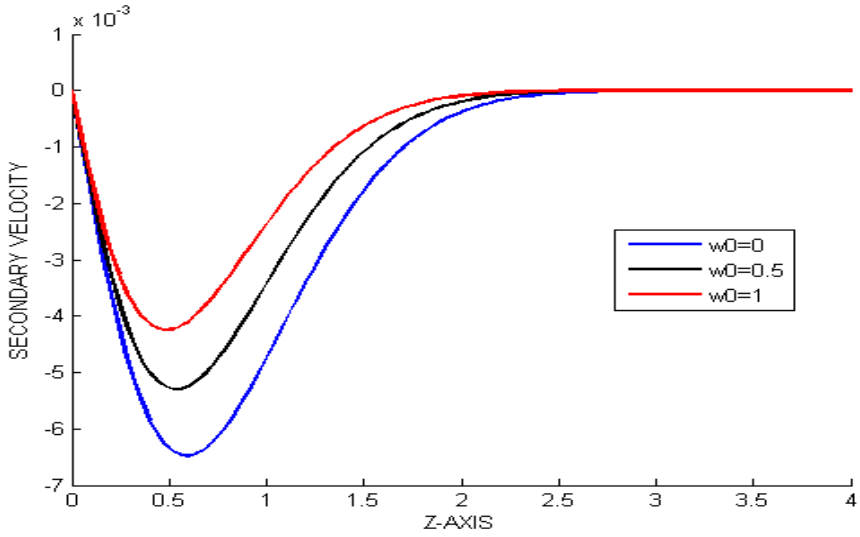

Figure 7.4b: Variation of Secondary velocity with Suction velocity $wo, Gr = -0.4$, with ion-slip

From figures 7.4a and 7.4b, we observe that;

i.) An increasde in Hall parameter or removal of suction velocity wo causes an increase in primary velocity profiles, this due to the fact that the effective conductivity decreases with the increase in Hall current parameter or removal of suction velocity which reduces the magnetic damping force hence the increase in primary velocity profiles.

ii.) An increase in Hall current parameter or removal of suction velocity profile causes a decrease in secondary velocity profiles, this is due to increase in the effective conductivity which increases the magnetic damping force hence the decrease in secondary velocity profiles.

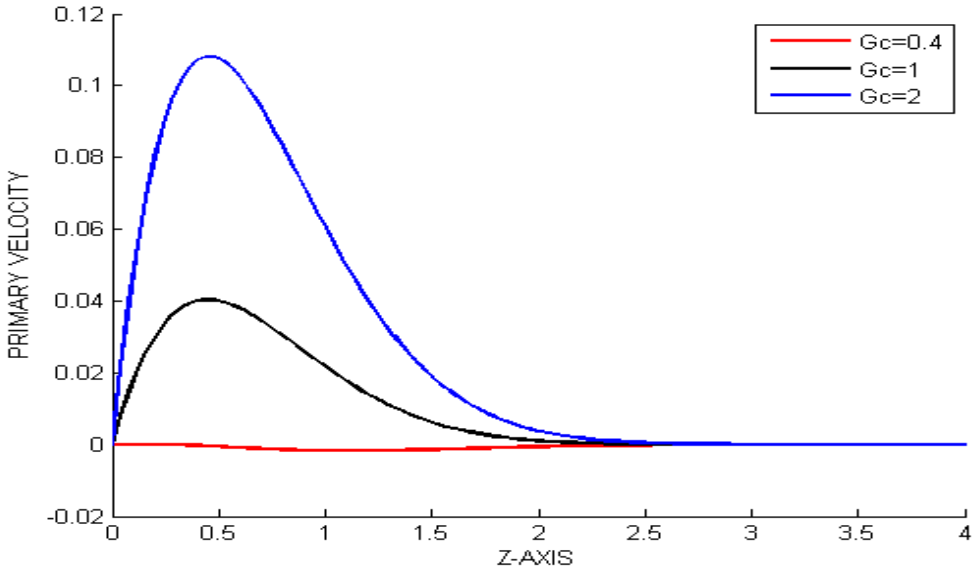

Figure 7.5a: Variation of Primary velocity with Modified Grashof $Gc, Gr = -0.4$, with ion-slip

Zain Publications
Company Registration No: UAN TS02E0015729
(Govt. of India, Ministry of Micro, Small & Medium Enterprises)
Contact Person: Dr. Mohd Zainuddin
Address: #12-1-898, North Lalaguda, Secunderabad, Telangana, India
Ngesa Joel Ochola, International Journal of Robotics and Information Technology, Volume 1, Issue 2, Dec 2017, Pg: 74-103

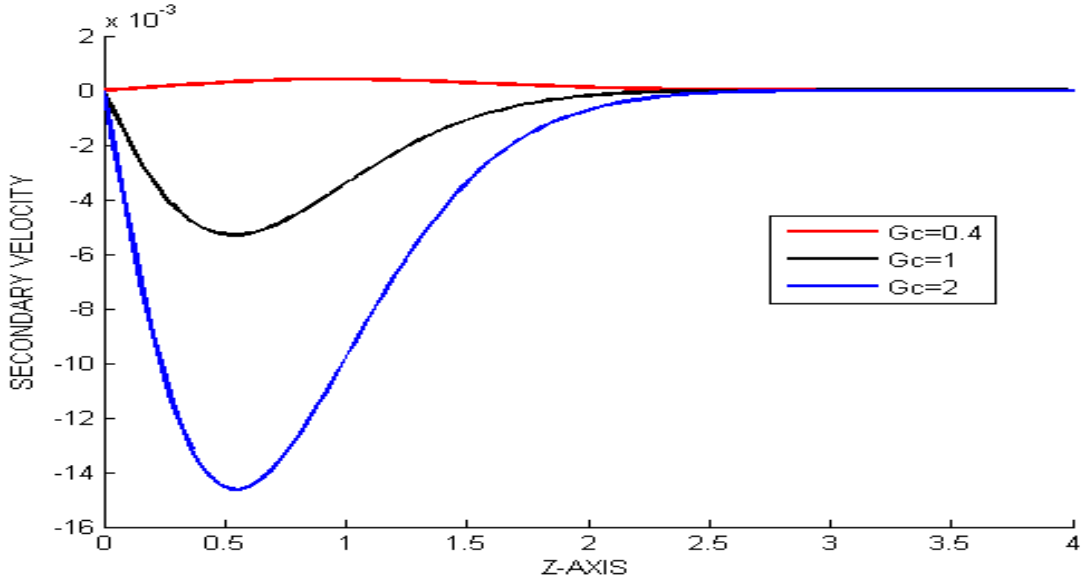

Figure 7.5 b:Variation of Secondary velocity with Modified Grashof $Gc, Gr = -0.4$, with ion-slip

From figures 7.5a and 7.5b, we observe that;

i.) An increase in modified Grashof number Gc causes an increase in primary velocity profiles but as the distance from the plate increases primary velocity profiles exhibit a decrease and remain parallel to the z-axis far away from the plate.

ii.) An increase in modified Grashof number Gc causes a decrease in secondary velocity profiles but as the distance from the plate increase secondary velocity profiles exhibit an increase gradually and remain parallel to the z-axis far away from the plate.

Conclusion

An analysis of the effects of various parameters on the velocities, temperature and concentration profiles on unsteady, free convection incompressible fluid flow past a semi- infinite vertical porous plate subjected to strong magnetic field inclined at an angle phi ψ to the plate with hall and ion-slip currents effects has been carried out. In all the considered cases, the applied magnetic field was resolved into two components and our work was restricted to the turbulent boundary layer.

In both cases of $Gr > 0$ and $Gr < 0$ it is observed that a thin boundary layer is formed near the stationary plate. The thickness of these boundary layers increases with increases in either Hall parameter m or ion-slip parameter.

. It was observed that in the absence of mass transfer and cooling or heating of the plate by free convection currents, increases in the Hall parameter m, the mass diffusion Sc, angle of inclination ψ, removal of suction velocity w_0 leads to no effect in temperature. An increase in heat source parameter σ leads to a decrease in primary velocity profiles but to an increase in

temperature profiles and secondary velocity profiles. For both $Gr > 0$ and $Gr < 0$ increases in the Hall parameter m, mass diffusion parameter Sc and removal of suction velocity w_o leads to decrease in primary velocity profiles.

For $Gr > 0$ increases in Hall parameter, angle of inclination, time and modified Grashof number leads to a decrease in secondary velocity profiles. Whereas increase in mass diffusion parameter Sc, heat source parameter and removal of suction velocity leads to an increase in secondary velocity profiles.

For $Gr < 0$ increase in mass diffusion parameter Sc and the removal of suction velocity leads to an increase in secondary velocity profiles but a decrease in primary velocity and concentration profiles. Increase in heat source parameter σ, angle of inclination, time and modified Grashof number Gc leads to an increase in primary velocity profile but a decrease in secondary velocity.

It was observed that an increase in the angle of inclination ψ or ion-slip parameter n causes an increase in primary velocity profiles and a decrease in secondary velocity profiles in both cooling and heating of the plate by free convection currents. Increases in Hall parameter leads to decrease in both primary and secondary velocity profiles. We also observed that increases in time leads to increase in both temperature and concentration profiles, but increase in heat source parameter, angle of inclination and removal of suction velocity causes decrease in temperature profiles.

REFERENCES

[1]. Benard K and Moreau R (2008). Magnetohydrodynamic Turbulence at low magnetic Reynolds," *Annual Review of fluid mechanics*" vol.40, pg.25-45.

[2]. Boffetta G , DeLillo , Mazzino A and Vozella L (2012).The ultimate state of thermal convection in Rayleigh-Taylor turbulence, "*Physical D: Nonlinear phenomenon*," vol.241, pg.137-140.

[3]. Bo Lu, Liangwang and Ziaonzhang (2013). Three Dimensional MHD simulation of the electromagnetic flow meter for laminar and turbulent flows. "*International Journal of Fluid flow*," Vol. 33, 239-243.

[4]. Chamkha, J.A, "Unsteady MHD convective heat and mass transfer past a semi-infinite vertical permeable moving plate with heat absorption." International Journal of Engineering and Science, vol.42, pp217-230, (2004).

[5]. Chaundhary R and Shin A. Direct Numerical simulation of transverse and span wise magnetic field effects on turbulent flow a 2:1 aspect ratio. "*International Journal MHD Turbulent fluid flow," Vol*. 27(2011), pg. 1123-1142.

[6]. Nakaharai H and Yokomine J (2007). Influence of a transverse magnetic field on the local and average heat transfer of an electrically conducting fluid." *International Journal of Heat and Mass transfer,"* Vol. 32 , pg. 23-28.

[7]. Rodriquez-Sevillano (2012). On the onset of turbulence in natural convection on inclined plates, *"Experimental Thermal and fluid Science*," Vol.35, pg.68-72.

[8]. Sanvicentre E, Giroux- Julien S, Menezo C and Bouia H (2013). Transitional natural convection flow and heat transfer in an open channel, "International *Journal of Thermal Sciences*," vol.99,pg. 215-224.

[9]. Satale S, Kunug T, Takase K and Ose Y (2006). Direct numerical simulation of turbulent flow under a uniform magnetic field for large-scale structures at high Reynolds number. "*Physical Fluids"* vol. 18, pg. 125-106.

[10]. Shin- ichi S, Chikamasa C, Kazuyuki M and Kunugi T (2010). Direct Numerical Simulation of unstable stratified turbulent flow under a magnetic field. "*International Journal of Heat and fluid flow,"* Vol.85, pg.

Zain Publications
Company Registration No: UAN TS02E0015729
(Govt. of India, Ministry of Micro, Small & Medium Enterprises)
Contact Person: Dr. Mohd Zainuddin
Address: #12-1-898, North Lalaguda, Secunderabad, Telangana, India

1326-1330.

[11]. Soundalgekar,V.M, Bhat,J.P, and Mohiuddin, M. "finite difference analysis of free convection effects on stokes problem for a vertical plate in a dissipative fluid with constant heat flux". International Journal of Engineering anmd Science, vol. 17, No. 12, pp 1283-1288,(1979).

[12]. Xenos M, Trirtzilaki E and Kafoussiass N (2009). Optimizing separation of compressible boundary-layer flow over a wedge with heat and mass transfer. *"International Journal of Heat and Mass transfer,"* Vol. 52, pg. 488-496.

[13]. Yamamoto Y (2008) DNS and k-ε model simulation of MHD turbulent channel flow with heat transfer," *International Journal of heat and mass transfer*," Vol. 28, pg.1-13.

[14]. Yoshinobu Y and Tomoaki T (2011). Heat transfer degradation in high Prandtl number fluid. "*International Journal of Heat and fluid flow," Vol.22*, pg. 67-83.

[15]. Zoynal M, Abedin M, Toshihiro T and Jinho L (2012). Turbulence characteristics and vertical structures in combined- convection boundary layers along a heated vertical flat plate, "*International Journal of heat and mass transfer*," vol.55, pg.3995-400.